Lorenzo Ferrari, BSc

State of the Art Analysis and Improvements of the Thermal Management System and the Transmission in Electric Vehicles

MASTER'S THESIS

to achieve the university degree of

Diplom-Ingenieur

Master's degree programme: Production Science and Management

submitted to

Graz University of Technology

Supervisor

Univ.-Prof. Dipl.-Ing. Dr.techn. Franz Haas

Institute of Production Engineering

Graz, December 2018

AFFIDAVIT

I declare that I have authored this thesis independently, that I have not used other than the declared sources/resources, and that I have explicitly indicated all material which has been quoted either literally or by content from the sources used. The text document uploaded to TUGRAZonline is identical to the present master's thesis.

24.01.2019
Date

Signature

Abstract

This thesis has the aim to answer the question of how an electric car will look like in the short future as ten years, in order to prepare the production for the upcoming needs. Particular focus is laid on the powertrain and the thermal management system. The trends are identified and the development of the required technologies is described. The main trend in the electric automotive industry is the downsizing. Smaller, high revving motors with a continuous increase of the power density have been the trend in the last decade. The downsizing of the motor requires a more performant and efficient transmission with an optimal gear reduction system. Battery packs become more and more powerful, requiring more performant cooling systems for the removal of heat.

List of acronyms

Acronym	Definition
AC	Alternating Current
BEV	Battery Electric Vehicle
CVT	Continuously Variable Transmission
DC	Direct Current
DOD	Depth of Discharge
EM	Electric Motor
E-CVT	Electronic Continuously Variable Transmission
EV	Electric Vehicle
FCV	Fuel Cell Vehicle
FHEV	Full Hybrid Electric Vehicle
HVAC	Heating Ventilation and Air Conditioning
ICE	Internal Combustion Engine
IM	Induction Motor
IPM	Interior Permanent Magnet
Li-ion	Lithium-ion
KERS	Kinetic Energy Recovery System
PHEV	Plug-in Hybrid Electric Vehicle
PMM	Permanent Magnet Motor
RMF	Rotating Magnetic Field
RPM	Revolutions per Minute
SEI	Solid Electrolyte Interphase
SI	International System of Units
SOC	State of Charge
SPM	Surface Permanent Magnet

List of symbols

Symbol	Designation	Unit
τ	Torque	N
k_1	Parameter defining the influence of input 1 on the output of the torque coupler	-
k_2	Parameter defining the influence of input 2 on the output of the torque coupler	-
ω	Rotational speed	rad*s^{-1}
q_k	Module of the heat flux by conduction	W* m^{-2}
k	Conduction heat transfer coefficient	W*m^{-1}*K^{-1}
∇T	Gradient of temperatures	K*m^{-1}
q_u	Heat transferred by convection	W
A	Area	m^2
h	Convection heat transfer coefficient	W*m-2*K-1
ΔT	Difference of temperatures	K
q_r	Heat transferred by irradiation	W
σ	Stefan-Boltzmann constant	W*m^{-2}*K^{-4}
ε	Emissivity	-
T	Temperature	K
$q_{gen,cell}$	Heat generation in a cell	W
I	Current	A
U	Theoretical open circuit potential	V
V	Cell potential	V
dU	Differential of circuit potential	V
dT	Differential of temperatures	K
m	Mass	Kg
dt	Differential of time	s
c_{cell}	Specific heat	J*K^{-1}*Kg^{-1}
Q_P	Power loss due to over potential	w
Q_S	Heat produced by the change of entropy	W
ΔS	Difference of entropies	Kg*m^2 *s^{-2}*K^{-1}
n	Charge number pertaining to the reaction	mol
Fa	Faraday constant	A*s*mol^{-1}
k_{heat}	Rate of the reaction producing heat	-
k_0	Frequency factor	-
E	Activation energy	J*mol^{-1}
R	Gas constant	J*K^{-1}*mol^{-1}
k_{cool}	Rate of the cooling system	-
λ_r	Conduction heat transfer coefficient in the radial-direction	W*m^{-1}*K^{-1}
λ_h	Conduction heat transfer coefficient in the height-direction	W*m^{-1}*K^{-1}
λ_d	Conduction heat transfer coefficient in the depth-direction	W*m^{-1}*K^{-1}

N_s	Synchronous speed	rad*s^{-1}
f	Frequency	Hz
P	Number of poles	-
v	Module of tangential speed	m*s^{-1}
r	Radius	m
F	Force	N
GR	Gear ratio	-
d	Diameter	m
m	Module of the gear	m
z	Number of teeth	-
a	Acceleration	m*s^{-1}
v_f	Final speed	m*s^{-2}
v_i	Initial speed	m*s^{-2}
F_T	Tractive force	N
F_R	Resistance force	N
Δt	Time span	s
r_{wh}	Radius wheel	m
r_R	Radius ring	m
r_S	Radius sun gear	m
r_P	Radius planet gear	m
ω_s	Rotational speed of the sun gear	rad*s^{-1}
ω_c	Rotational speed of the sun gear	rad*s^{-1}
Z_R	Number of teeth of the ring	-
Z_s	Number of teeth of the sun gear	-
Γ	Parameter of the teeth of the planetary gearing	-
ω_{SC}	Difference of the rotational speed of the sun gear and carrier	rad*s^{-1}
ω_{RC}	Difference of the rotational speed of the ring gear and carrier	rad*s^{-1}
ω_C	Rotational speed of the carrier	rad*s^{-1}
$P_{E-CVT,out}$	Power in output from the E-CVT	W
P_{IC}	Power generated by the IC	W
P_{EM}	Power generated by the IC	W
$\omega_{E-CVT,out}$	Rotational speed of the output axle of the E-CVT	rad*s^{-1}
ω_{IC}	Rotational speed of the input axle of the E-CVT coming from the IC	rad*s^{-1}
ω_{EM}	Rotational speed of the input axle of the E-CVT coming from the EM	rad*s^{-1}
$\tau_{E-CVT,out}$	Torque of the output axle of the E-CVT	N*m

Table of contents

1 Introduction: The steps of the electrification of the automotive industry in the last two centuries

Over the last years, the automotive industry has experienced the emergence of a new trend: electrification. The more and more evident signs of the climate change together with the increase of the value of the air pollutants, especially in urban areas, can be identified as triggers for the production and selling of electric cars.

Electric power used to power a vehicle is indeed not a new technology. In fact, the first-prototypes of electric vehicles date back to the 19th century. The development of the electric motor is strictly correlated with the discovery and the exploration of electromagnetism and electrochemistry.

During the second half of the 18th century, Luigi Galvani an Italian physicist, carried out experiments involving electricity. He experimented a flow of energy once a leg muscle of a frog is touched at different points at the same moment with different materials. He wrongly supposed that the electricity was coming from the animal. Alessandro Volta starting from Galvani's studies carried out experiments showing that biological elements are not needed to produce electricity. He produced a cell which was able to generate electricity, made by two disks of different metals separated by an electrolyte material. Alessandro Volta is credited with the invention of the first electrical battery in the first years of the 19th century. The battery, named after him Voltaic Pile, was made from alternating disks of zinc and copper, with a textile element impregnated with an electrolyte solution, like salt water in between. He assumed that the source of electricity was in the physical properties of the metals. A couple of decades later, Michael Faraday, a British scientist operating in the electrochemistry and electromagnetism fields, proved that the source of electricity was chemical by nature and that it was generated by the interface of the two electrodes with the electrolyte. These discoveries were setting the basis for the development of the batteries and boosted the interest of researchers in electricity.[1] [2] [3]

In the following years, several discoveries in the electromagnetic fields were made. Hans Christian Ørsted, in 1820, understood the existence of a correlation between magnetism and electricity by observing the interaction between a compass and an electrified wire. One year later, Faraday invented a homopolar motor (a direct current electric motor with two magnetic poles). André-Marie Ampère discovered in the same year that a current-carrying wire with a helix shape acts like a magnet. Still in 1821, William Sturgeon built the first electromagnet, by wrapping a coil around a U-shape beam of iron. A further improvement on the electromagnet was done by Joseph Henry who insulated the wires; he also discovered that current flow can be generated by a change in magnetism.[4] [5]

In 1831, Joseph Henry developed an experimental motor made by a straight electromagnet which could rotate in the horizontal plane, see figure 1. With the oscillation of the beam, the wires, wrapped around the iron beam, were changing the connection with the electrochemical cells, and hence, the polarity was switching. A rotary motor was prototyped a couple of years later by William Sturgeon, and

[1] Conf. Arnott (1877), p. 716-721.
[2] Conf. The Editors of Encyclopaedia Britannica (2018), online source [accessed on 11 November 2018].
[3] Conf. Whelan; Reilly; Rockwell (2014), online source [accessed on 11 November 2018].
[4] Conf. French (2017), p. 82-88.
[5] Conf. Miller (2001), p. 7-9.

together with it the commutator, a rotary device which provides the polarity switching and hence, reverse the current direction. This was setting the basis for the DC motor. [6]

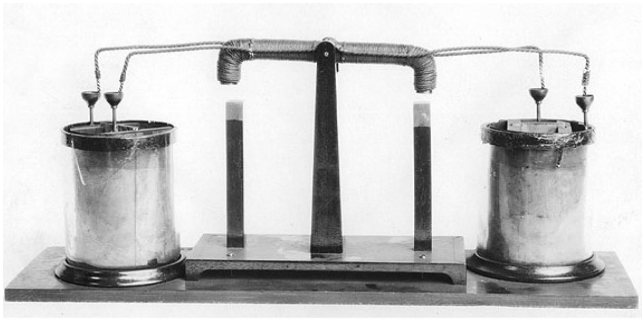

FIGURE 1: JOSEPH HENRY'S OSCILLATING MOTOR, ONLINE SOURCE: EDISON TECH CENTER, [ACCESSED ON: 21 NOVEMBER 2018]

Moritz Hermann Jacobi developed an electric motor with a mechanical power of around 15W in 1834, and sent a detailed report to the Academy of Sciences of Paris explaining his invention. He was awarded an honorary doctorate to pay tribute to his studies by the University of Königsberg. In the following years, Jacobi kept doing experiments in the field of electromagnetism. As he was interested in the successful research of Jacobi, the Russian tsar invited him to join the St. Petersburg Academy of Science. Jacobi accepted, and, with the funding of the Academy, he developed a 300W motor in 1838 (see figure 2). The application of this electric motor was demonstrated by powering an 8-meter-long boat with paddle wheels. The energy was stored in zinc batteries which reached a weight of 200 kg. This multipolar engine was provided with 24 electromagnets divided into two stationary wooden structures with alternated polarity. A rotary part was placed in between, it was carrying another set of electromagnets. The motion of this part was generated by the attraction and repulsion with the fixed electromagnets. The polarity of the rotating electromagnets was inverted by using a commutator in order to keep the motor rotating. [7]

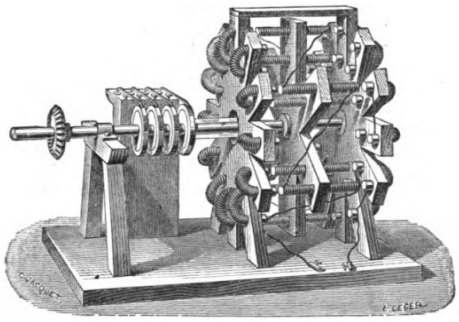

FIGURE 2: IMPROVED VERSION OF JACOBI´S 300W MOTOR DEVELOPED IN 1838, BASED ON ONLINE SOURCE: ETI KIT, [ACCESSED ON: 21 NOVEMBER 2018]

[6] Conf. Whelan; Reilly; Rockwell (2014), online source [accessed on 21 November 2018].
[7] Conf. KIT (2018), online source [accessed on 21 November 2018].

On the other side of the Atlantic Ocean, in 1837, Thomas Davenport, a blacksmith from Vermont, patented an electric motor. It was the first American patent on an electric motor which was able to do real work. Davenport used to read the "American Journal of Science and Arts", the journal on which Joseph Henry used to public articles explaining his discoveries. It is likely that Davenport was influenced by Henry's prototypes, in fact the first motor that Davenport patented was reversing its polarities by the rotation of the motor. His model was working with a rotational part on which four electromagnets were fitted and a stationary part with permanent magnets. After having applied for the patent, he kept improving the design. Six months later, a new version of his prototype was spinning at one thousand revolutions per minute and was able to generate around 4.5W power.[8] [9]

At the same time, in Scotland, Robert Davidson was working on electric motors. In 1842, after several prototypes he developed an electric locomotive with a weight of around 7000 kg. It was powered by two reluctance motors which enabled the machine to reach the speed of 6.4 km/h. The energy was provided by a set of zinc-acid batteries.[10]

In 1856**,** Werner von Siemens built an electric machine in which the windings are set into slots with a double T armature, see figure 3. This design has been adopted since then for almost all electric motors.[11]

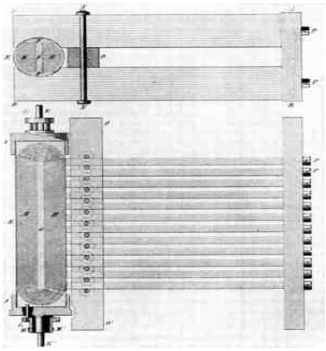

FIGURE 3: ARMATURE DOUBLE T WITH SLOTS FOR WINDINGS DEVELOPED BY SIEMENS, ONLINE SOURCE: ETI KIT, [ACCESSED ON: 21 NOVEMBER 2018]

So far, the motors had been using energy stored in zinc batteries. However, this technology was expensive and could not compete with the costs related to the steam engine. According to R. Hunt, the cost of the power required by a steam engine was about 25 times less than the one required by an electric motor.[12]

The second half of the 19th century was prolific in inventions in the battery technology field. In 1859, the French physicist Raymond Gaston Planté invented the rechargeable lead-acid battery. This battery was made of a lead anode and a lead dioxide cathode designed as spiral-wound plates separated by rubber strips, submerged in a sulphuric acid solution. The chemical reaction produces electrons at the

[8] Conf. Schiffer (2013), p. 88-90.
[9] Conf. KIT (2018), online source [accessed on 21 November 2018].
[10] Conf. Day; McNeil (1998), p. 340.
[11] Conf. KIT (2018), online source [accessed on 21 November 2018].
[12] Conf. KIT (2018), online source [accessed on 21 November 2018].

anode while at the cathode they are consumed, hence current is produced. By passing a reverse current, the battery can be recharged. After a couple of decades, in 1880, Camille Alphonse Faure improved Planté ´s invention. The lead plates were treated with a water solution of sulphuric acid and lead oxides, generating a coat of lead sulphates on the plates. This treatment led to a higher capacity of the battery. Using rechargeable batteries, Thomas Parker invented the first real-sized electric-driven automobile in 1884. [13] [14]

Two inventors started, although independently, almost at the same time working on induction motor prototypes: Nikola Tesla and Galileo Ferraris. In the subsequent two paragraphs, Boldea and Nasar (2002) are quoted. The text refers to Tesla and Ferraris. It tells the story of their first inventions and a later development of a three-phase motor done by Dolivo-Dobrovolsky. [15]

Nikola Tesla, a Serbian-American inventor, was the first one working and experimenting on multi-phase systems and induction phenomena. He was developing these concepts already in 1882 while studying in Graz, Austria. Independently from the work of Tesla, Galileo Ferraris, an Italian scientist invented in 1885 an induction machine. About one year later, Tesla patented in the US an induction motor as well. The different prototypes of Ferraris and Tesla were running with two-phase alternating current. On the ferromagnetic stator core, there were wrapped the windings 1-1' and 2-2' running with different phases, as shown in figure 4. The rotor of Tesla's machine was provided with short-circuited windings and was made of ferromagnetic material. The rotor of Ferraris' machine was made in copper. In both machines the rotor had a cylindrical form.

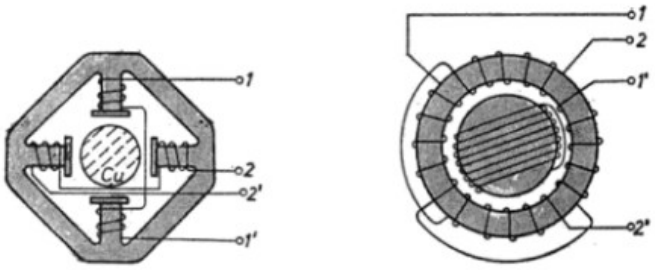

FIGURE 4: AT THE LEFT FERRARIS' PROTOTYPE (1885), AT THE RIGHT TESLA'S ONE(1886), SOURCE BOLDEA, NASAR (2012), P. 2

The concept of the induction motor has remained the same. The principle is that a magnetic rotating field is produced by the multi-phase windings, and the magnetic field induces a current in the close windings of the rotor. The interaction between this current and the field produces torque. Between the years 1889 and 1991 the Russian, naturalized Swiss, Mikhail Osipovich Dolivo-Dobrovolsky was doing experiments on polyphase electrical devices. He is credited with the invention of the three phase-cage induction motor the wound rotor and the slip ring for three-phase induction motor with starting resistors.

[13] Conf. Pavlov (2011), p. 4-12.
[14] Conf. Mackay (2011),p. 20.
[15] Conf. Boldea; Nasar (2002), p. 2-3.

The first two decades of the 20th century are considered as a "golden age" of the electric vehicles in the USA. At that time three different technologies could power a vehicle: an internal combustion engine, a steam engine or an electric motor. By the year 1900, steam engine vehicles were the most sold with 1681 pieces, followed by the electric vehicles with 1575 sold and last the gasoline engine with 936. Advantages of the steam powered vehicles were the price and the speed. The electric vehicles were equipped with batteries, they represented the most clean and silent solution of all three; one disadvantage was their short autonomy range, although at that time roads existed mainly in the cities and hence the normal trip of a vehicle was not an issue for this type of powertrain. The internal combustion vehicles could travel longer distances with good speed performance, but they were dirtier and more difficult to start. Till the year 1920**,** no technology managed to prevail in the USA. In the following years the internal combustion engine became the best sold. One reason was that the network of roads between the cities became better, thus the need of vehicles with a good autonomy range increased. Another cause was the mass production of the Ford Model T. This model was the first one produced according to the mass production principles of Henry Ford. The idea of Henry Ford was to produce a highly standardised and widely affordable vehicle. The price dropped from 850 USD in 1909 to 260 USD in 1920. The Model T was an enormous success and made popular the vehicles powered with combustion engines. In the same years petrol prices dropped from around 48 cents for a gallon to around 15 cents in 1928. For all these reasons, the vehicle scenario for the rest of the 20th century was dominated by the ICE. [16] [17]

During the 1970s, two oil crises shocked the world. The first one in 1973 when some countries in the Middle East decided to stop supplying oil to the countries who supported Israel during an Arab-Israeli conflict. The second crisis started in 1979 and was connected to a revolution in Iran. The oil crises led to a suddend and substantial increase of the oil prices.[18]

These crises raised concerns on petrol as energy source for vehicles. Automobile manufacturers like Nissan, Ford and General Motors developed in the 70s and 80s prototypes of electric cars. Even if the motor technology could satisfy part of the customer, the biggest problem stayed in the battery pack cost and the autonomy range. [19]

In the last decades of the 20th century, deep concerns regarding pollution and global warming arose and pushed governments to launch countermeasures. One of the most important international treaties of those years was the Kyoto Protocol. It was signed in December 1997 and was aiming at a reducion of greenhouse gas emissions.[20] National initiatives to find alternatives for ICE vehicles emerged worldwide. At the beginning of the 21st century researchers indentified fuel cells as an adeguate technology to replace the ICE. Almost in parallell the research improved the performance of lithium batteries. Today the increasing use of EVs is mainly due to political measures such as various financial incentives for EVs and transit bans in urban areas for certain categories of ICE vehicles. The production of EVs and plug-in hybrids (PHEVs) is growing fast: in the first half of 2018 there was a worldwide increase by 66% compared to the same period of 2017. BEVs were the most sold with a share of 64% whilst the share of PHEVs was 36%. With a market share for EVs of 51%, China is the country with the highest volume of EVs sold in the first half of 2018. Figure 5 shows a chart regarding

[16] Conf. The AA Motoring Trust (2005), p. 1.
[17] Conf. Ajanovic (2015), p. 521-524.
[18] Conf. Venn (2002), p. 7-29.
[19] Conf. Anderson; Anderson (2010), p. 49-50.
[20] Conf. United Nations Climate Change (2018).

the EVs in circulation over the last four years, at the time of writing. It can be observed how the trend of sales has been growing quickly especially in China, where the number of EVs in circulation in 2013 was 0.03 million whilst it was 1.23 million in 2017. In the USA, in the same period, the number of EVs in circulation increased from 0.17 to 0.76 million and in Europe from 0.1 to 0.82 milion. [21] [22]

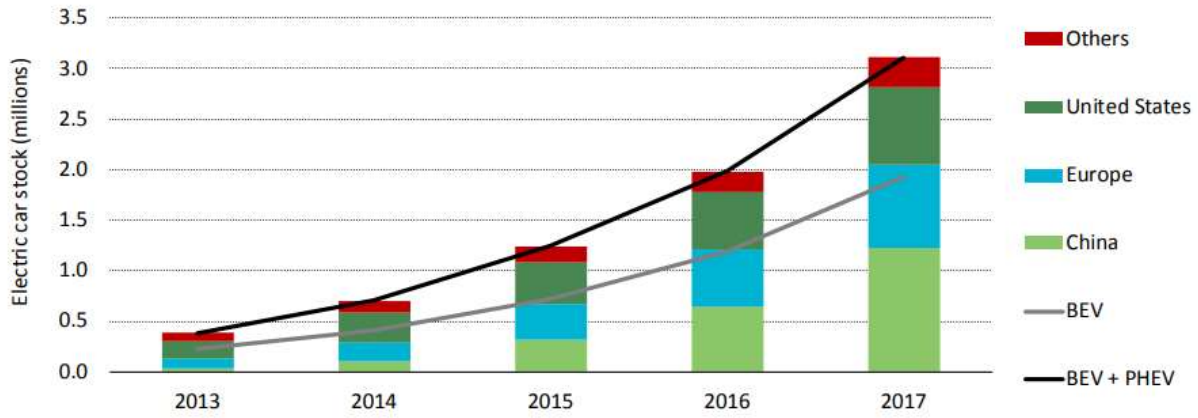

FIGURE 5: NUMBER OF ELECTRIC VEHICLES IN CIRCULATION, SOURCE: INTERNATIONAL ENERGY AGENCY (2018), P.9

The internal market share is a relevant indicator to understand the sales of EVs nowadays: it shows the percentage of EVs relative to the total of vehicles that were sold that year in that country. Quoting the IEA Global Electric Vehicle Outlook 2018, Norway with over 39% was the country with the highest share, followed by Iceland (11.7%), Sweden (6.3%), China (2.2%) and Germany (1.6).

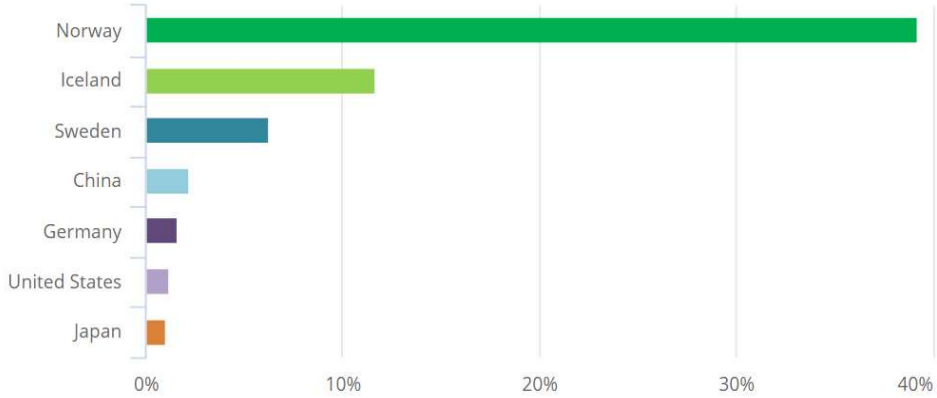

FIGURE 6: INTERNAL MARKET SHARE OF ELECTRIC CARS, ONLINE SOURCE: INTERNATIONAL ENERGY AGENCY, [ACCESSED ON: 11.11.2018]

[21] Conf. EV Volumes (2018), online source [accessed on 11.11.2018].
[22] Conf. International Energy Agency (2018), online source [accessed on 11.11.2018].

Forecasts predict exponential growth in the electrification of vehicles. The following charts are taken from the Global EV Outlook 2018 of the International Energy Agency. They display two different scenarios. One is called New Policies Scenario and is based on the current and announced policies. The other one is called EV30@30 Scenario. It predicts an enhanced focus on electric vehicles on the part of governments and it therefore displays more ambitious targets. According to the first chart, in 2030 the number of EVs on the road will go up to 125 million, the second one foresees 220 million. It is interesting to note that according to the EV30@30 Scenario, the BEVs on the road will be more than the PHEVs, whereas the New Policies Scenario foresees that the PHEVs will hold a higher share than BEVs.[23]

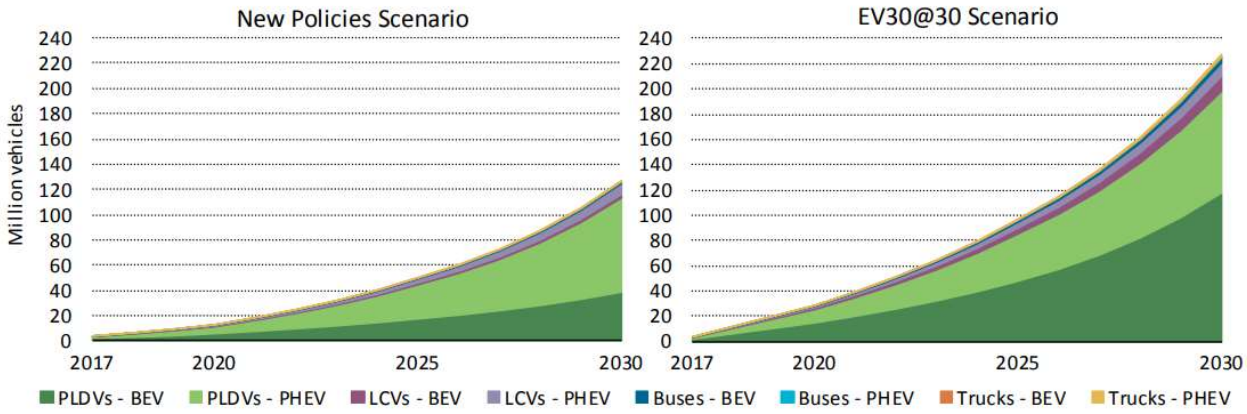

Notes: PLDVs = passenger light duty vehicles; LCVs = light commercial vehicles; BEVs = battery electric vehicles; PHEV = plug-in hybrid electric vehicles.

FIGURE 7: FUTURE SCENARIOS OF EVS ON THE ROAD, SOURCE: INTERNATIONAL ENERGY AGENCY (2018), P. 12

In addition to government policies, a trigger for a greater incitement to purchase BEVs is the improvement of the infrastructure of charging stations. Charging stations allow to recharge the batteries of BEVs. The time required for this process is determined by the charging power and the battery capacity. The so called “Supercharger” of Tesla delivers around 140 KW and under optimal conditions it is able to recharge an 85 KWh Tesla S from 0% to 80% in 40 minutes. When approaching to the full energy capacity of the batteries, the charging power decreases so as not to damage them[24]. The Supercharging service is not widespread; in Austria at the time of writing there are 16 stations of Superchargers[25]. The Chinese automotive manufacturer NIO has developed a different solution to provide BEVs rapidly with electricity. NIO has been setting up swap stations along Chinese highways: NIO EVs drive in, the battery of the vehicle is taken off by robots and replaced by a fully charged one in around two minutes. The battery packs are located on the bottom of the vehicle and are standardised in order to be removed easily by robots. The company aims to set up 1100 of these stations by 2020.[26]

[23] Conf. International Energy Agency (2018), p. 11.
[24] Conf. Yamauchi (2018), online source [accessed on 11.12.2018].
[25] Conf. Tesla (2018), online source [accessed on 11.12.2018].
[26] Conf. Holzer (2018), online source [accessed on 11.12.2018].

2 Classification of vehicles based on level of electrification

It is possible to classify EVs on the basis of the amount of power delivered by the electric motor/motors (EM) and the possible presence of other engines, such as internal combustion engines (ICEs). Vehicles, which are equipped with ICE and EM technologies are called hybrids. It is possible to speak about level of hybridisation or electrification referring to the amount of power produced by the EM compared to the one produced by the ICE.

A possible classification is proposed by Riemenschneider and Lienkamp: they propose to use as a descriptive parameter the contribution of the electric motor compared to the one produced by the internal combustion engine as shown in figure 8. In this diagram the different levels of vehicle electrification are displayed related to time, as description of their market entrance and development.[27]

The first level, the "Improvement of ICE / micro hybridisation" describes the lowest level of electrical contribution to the propulsion systems. Technologies such as Stop/Start, regenerative braking and starter generator may be present in vehicles of this level. Stop/Start is a system that switches off the motor when the velocity of the vehicle is zero and the vehicle is in neutral. The car is restarted once a gear is re-engaged. A higher number of starts and stops leads to a higher utilisation of the battery and a decrease of fuel consumption especially in urban areas. Regenerative braking is a device that converts kinetic energy, in energy to recharge the battery. The starter generator replaces the starter of the motor and the alternator. It is installed between the engine and the transmission and it operates both as Stop/Start system and regenerative braking, an additional battery is installed for this device.[28]

In contrast to in the micro hybridisation, in the mild level, electrical involvement occurs in the drivetrain. Vehicles of this level may be equipped with passive boosts. This device carries out the function of the starter generator and recovers kinetic energy. To perform the latter one, the device reverses the polarity of the generator transforming it into a motor and it is connected to a high voltage battery, ultra-capacitors or a flywheel, which can be used to boost the acceleration. This concept was first introduced in Formula 1 race cars as KERS. [29]

In full hybrid vehicles, the electric motor can power the vehicle by itself, but only for modest distances. A high-power starter generator is provided and it is decoupled by an additional clutch from the ICE and the transmission. [30] [31]

Plug-in hybrid vehicles are equipped with a battery pack and a socket for external charging. Pure electric driving is possible, although for minor distances, usually around 100 kilometers. It is a technology that allows short distances to be driven with zero local emission. The problem of short

[27] Conf. Eckl et al. (2013), p. 122-123.
[28] Conf. YUASA (2014), online source [accessed on 14.12.2018].
[29] Conf. YUASA (2014), online source [accessed on 14.12.2018].
[30] Conf. Eckl et al. (2013), p. 122-123.
[31] Conf. YUASA (2014), online source [accessed on 14.12.2018].

autonomy ranges is avoided since the vehicles are equipped with an ICE as well. This technology might be considered the transition between the predominance of ICE vehicles over EVS. [32]

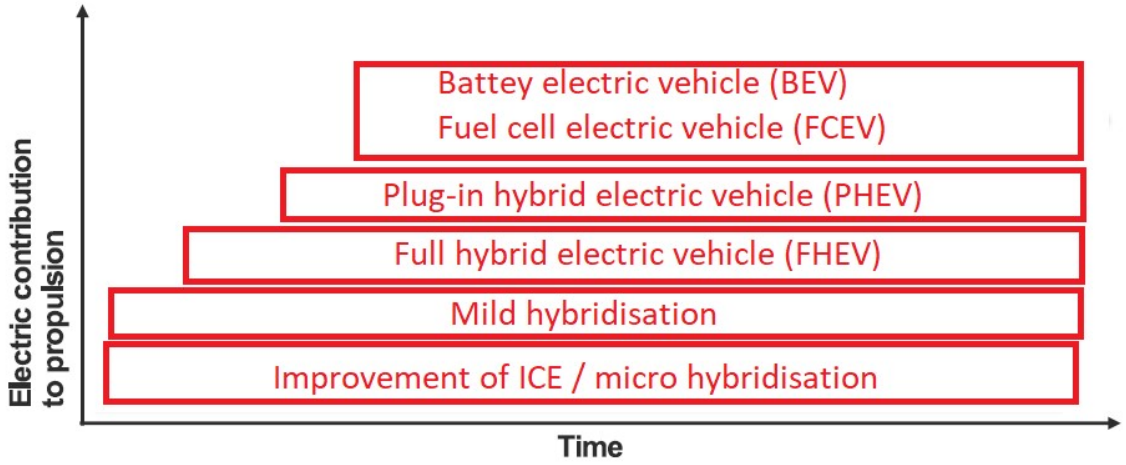

FIGURE 8: LEVELS OF VEHICLE HYBRIDISATION, BASED ON ECKL (2003), P. 123

Speaking about the highest level of electrification, it is possible to distinguish between BEVs and FCVs (fuel cell vehicles). In the first ones, the energy to power the electric motor is stored in a battery back and the main recharging process is performed by plugging it into an external electric power source. In the second ones, a fuel cell produces electrical energy that can be stored.

Both fuel cells and batteries transform chemicals into electricity. The two technologies display some differences. In the fuel cell the chemicals are provided by an external storage system to the cell where the electrochemical oxidation occurs. The reaction continues while fuel and oxygen are supplied. Generally, FCVs use compressed hydrogen in storage-devices and air from the atmosphere. In the fuel cell the electricity is produced by oxidation of the fuel at the anode and the reduction of the oxygen at the cathode. Whereas, the battery has, however, a limitation. Its capacity is due to the fact that the reaction takes place in the same device where the chemicals are stored, hence it is not possible (or more precisely, it is not designed) to supply new chemicals. When the battery circuit is closed, the reaction occurs and electrons are flowing from the anode to the cathode. Once the chemistry at the anode has released all its electrons or if the system is unable to continue the chemical reaction, the flow of electrons will be interrupted. Batteries used to power vehicles are rechargeable nowadays. This process is done by providing DC current to the battery. The battery behaves as an electrolytic cell during the recharging process. Fuel cells are often used in combination with a traction battery, which is recharged by the electrochemical process of the fuel cell and the regenerative braking system. The

[32] Conf. Eckl et al. (2013), p. 122-123.

battery can provide energy in high-power demand situations and improve its total efficiency. If fuel cells are used in combination with other power sources, those vehicles are referred to as hybrids. [33] [34]

Compared to li-ion batteries, hydrogen powered FCVs have a better energy to weight ratio and a fast refilling process (comparable to the gasoline one). A disadvantage are the costs: hydrogen is expensive to produce, it is mainly obtained from water by electrolysis, the process is energy-intensive and can absorb up to half of the energy obtained. Further drawbacks are the storage and transportation of the hydrogen. Hydrogen is highly inflammable and the material of the tanks has to be inert in order to avoid breakages.[35]

It is possible to classify the hybrid powertrain in three categories of layouts: series hybrids, parallel hybrids and series-parallel hybrids. This definition sets out how the power, coming from different sources, is merged (or not) before reaching the final drive (or final transmission).

In the series-parallel drivetrain only the electric motor is used to power the driving wheels. A fuel tank provides gasoline to the ICE, which uses the energy to power itself and an electric generator. The electricity produced by the generator traverses an electronic AC/DC converter and then it is used to charge the battery. The second source of energy is the battery pack. The energy of this pack traverses a DC/DC converter in order to adjust the voltage according to the requirements of the electric motor. The torque and speed in output from the electric motor are applied then to the final transmission. The electric motor can be used as a generator to recharge the battery during the regenerative braking phase.[36]

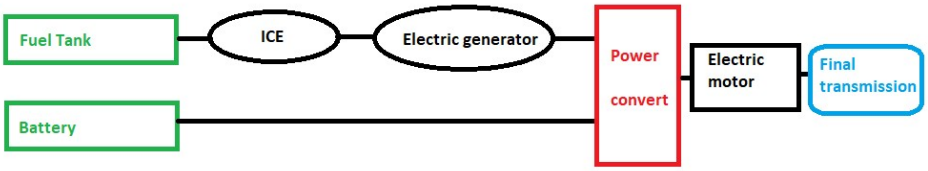

FIGURE 9: SERIES HYBRID ARCHITECTURE SCHEME, BASED ON: CORBELLI (2011), P. 24

In the parallel hybrid architecture both power sources can power the driving wheel. The power of the battery is flowing into the electric motor directly passing the DC/DC converter. It is then merged to the one coming from the ICE in the gearbox. Conversely on the series hybrid, where the powers are coupled together electrically, in the parallel hybrid architecture, it happens in a mechanical way through the gearbox.[37]

[33] Conf. Corbo et al. (2011), p. 71.
[34] Conf. Toyota (2018), online source [accessed on: 22.11.2018].
[35] Conf. Wertheimer (2018), online source [accessed on 11.11.2018].
[36] Conf. Corbelli (2011), p. 25.
[37] Conf. Corbelli (2011), p. 26.

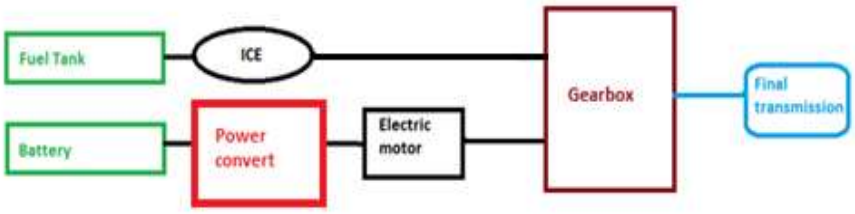

FIGURE 10: PARALLEL HYBRID ARCHITECTURE SCHEME, BASED ON: CORBELLI (2011), P. 24

In case more power is needed instantly for a short time (i.e. to accelerate), it is possible to get it from the engine. A disadvantage is that the engine has to accelerate to match the speed of the wheels, hence it is not always in the band of maximum efficiency. As mentioned before, it requires a more complex architecture since the two power sources are linked together at the gearbox. A clutch system is a possible solution for this problem. To couple the two power paths a torque coupling or a speed coupling are possible. In the torque coupler, the torque (τ_{out}) is a linear combination of the input torques ($\tau_{1,in}$, $\tau_{2,in}$) based on the parameters k_1 and k_2 as explained in equation (3.1) not including losses, and the output speed is obtained as shown in equation (3.2). [38]

$$\tau_{out} = k_1 * \tau_{1,in} + k_2 * \tau_{2,in} \quad (3.1)$$

$$\omega_{out} = \frac{\omega_1}{k_1} = \frac{\omega_2}{k_2} \quad (3.2)$$

In the speed coupler the output speed (ω_{out}) of the shaft is a linear combination of the two in input ($\omega_{1,in}$, $\omega_{2,in}$). By excluding losses, it is possible to describe it with equation (3.3) and the output torque is derivable as in equation (3.4) .[39]

$$\omega_{out} = k_1 * \omega_{1,in} + k_2 * \omega_{2,in} \quad (3.3)$$

$$\tau_{out} = \frac{\tau_{1,in}}{k_1} = \frac{\tau_{2,in}}{k_2} \quad (3.4)$$

Compared to parallel hybrid, series-parallel hybrid architecture has the advantage that the engine is not coupled to the wheels, so it can operate at the most efficient point. A drawback of the series architecture is that all power has to come from the motor to the wheel, it is not possible to use the ICE in situations where more power is needed. Another disadvantage is related to the inefficiencies. Energy conversion leads to losses due to the ICE, the electric generator and the charging of the battery.

[38] Conf. Corbelli (2011), p. 27.
[39] Conf. Corbelli (2011), p. 28.

The series-parallel hybrid is a combination of the previous seen two architectures and aims to merge the benefits of both of them. Thanks to the power split, it can run the vehicle using the power of both the ICE and EM, or just one of them depending on the driving conditions. While the ICE is running, the power management unit combining the power of the EM, keeps the ICE at the most efficient rate possible.[40]

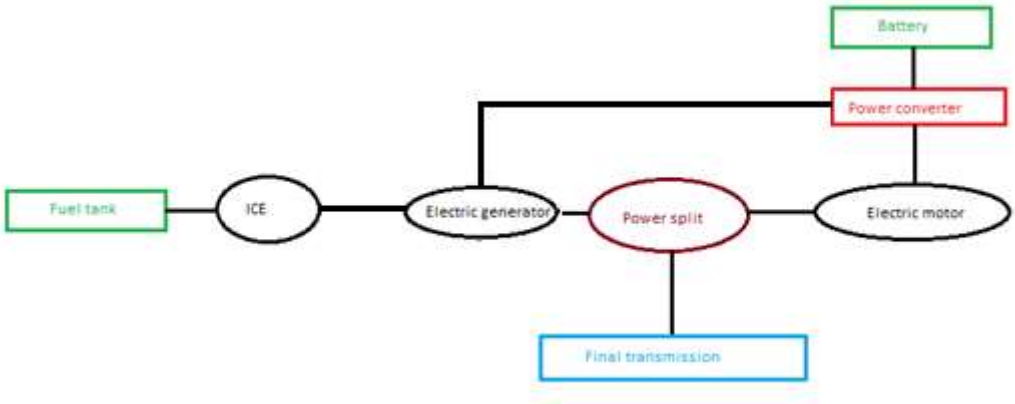

FIGURE 11: SERIES-PARALLEL HYBRID ARCHITECTURE SCHEME, BASED ON: CORBELLI (2011), P. 24

[40] Conf. Fayyad et al. (2012), p. 146-147.

3 Thermal management systems

The term “thermal management system” is used to designate all the devices used to keep the temperature of different parts of the vehicle in a specific range. This range can be the one to allow the components to work well or to guarantee the comfort required for the passengers.

3.1 Introduction to the thermal management systems

It is possible to identify several thermal management system areas for a vehicle. In electric vehicles five different main parts have to be considered while designing the cooling systems: the battery pack, the electronic, the motor, the transmission and the cabin.

Regarding electric vehicles, a specific focus is on the cooling of the battery. The battery coolant systems have to keep the battery pack in a specific range of temperature. This range depends on the battery technology used. Other parameters which have to be taken into consideration while designing the cooling system of the battery pack are the type and number of cells used and how they are grouped. Chapter (3.3.1) will cover this aspect in detail.

The heat flux in the electric motor is strongly dependent on which type of technology is adopted. The most two common nowadays are the induction motor (IM) and the permanent magnet motor (PMM). The cooling requirements of IMs are based on the limit working temperatures of the windings (usually in copper or aluminium), whereas the ones for PMMs are about the critical temperature of the magnets.

The performances of the motor are proportional to the electric current which is powering the engine. However, the amount of current in the windings can be increased only within the range imposed by the materials. Cooling stator and rotor influence directly the lifetime of electric motors, the output capability and their reliability. The trends nowadays push the motor towards downsizing on the one hand and increased performance on the other hand, thus the heat fluxes rise and the engine needs higher cooling performance.[41]

The cooling/heating for the cabin has to be designed in order to guarantee the comfort of the passengers. The perception of the thermal comfort depends on several factors, this argument is further discussed in paragraph 3.5. [42]

[41] Conf. Tong (2014), p. 409.
[42] Conf. Simion; Socaciu; Unguresan (2016), p. 472-478.

3.2 Heat transfer methods

Energy conversion processes can generate or be the result of heat transfer phenomena. The mechanisms of heat transfer are conduction, convection and radiation. Conduction occurs by molecular interaction, whereas convection by fluid motion and radiation describes the heat exchange via electromagnetic waves. The direction of the heat flux is given by the temperature difference: heat flows towards the lowest temperature. Heat transfer mechanisms follow the principle of energy conservation and describe the difference of temperature in spatial and time variation. According to the principle of energy conservation the sum of flows of energy and heat across a control system (mass or volume) with the work done on the system and the energy converted and stored in it, is zero. [43]

Fourier´s conduction formula is reported in equation (3.5) where q is the heat flux (W*m^2), k is the material conductivity coefficient (W*m^{-1}*K^{-1}) and ∇T is the temperature gradient (K*m^{-1}). The convection heat transfer mechanism follows equation (3.6), where h is called the convection heat transfer (W*m^{-2}*K^{-1}), A (m^2) represents the area of heat exchange and ΔT is the temperature difference of the entities considered. Equation (3.7) explains the Stefan-Boltzmann law on how heat is generated through irradiation, the constant σ has a specific value of 5.67*10^{-8} W*m^{-2}*K^{-4}, ε is called emissivity and is a coefficient, which varies from 0 to 1m and describes the radiative property of a surface.[44]

$$q_k = -k * \nabla T \tag{3.5}$$

$$q_u = h * A * \Delta T \tag{3.6}$$

$$q_r = \sigma * \varepsilon * T^4 * A \tag{3.7}$$

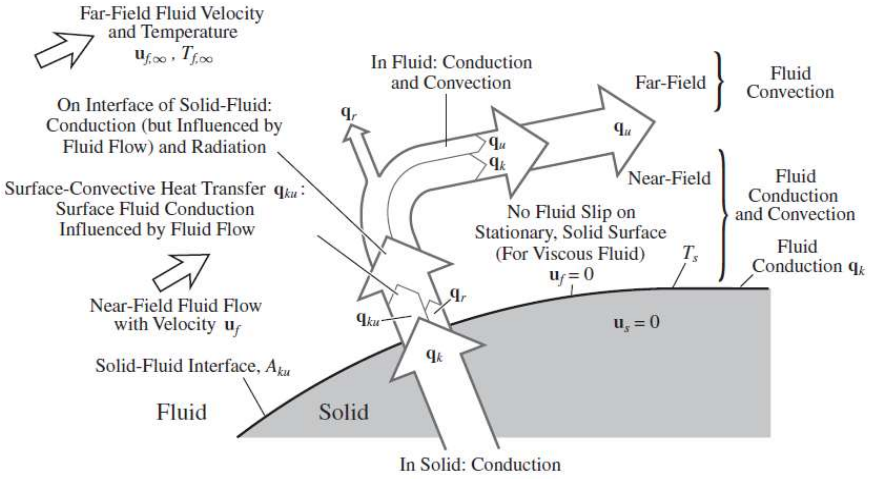

FIGURE 12: EXCHANGE OF HEAT MECHANISM FROM A SOLID TO A FLUID, SOURCE: KAVIANY (2011), P. 427

[43] Conf. Kaviany (2011), p. xviii, 152, 433.
[44] Conf. Rathore (2010), p. 1025-1027.

3.3 Battery-packs

The most important goals for the development of batteries for BEVs are to reduce costs and to increase the driving range capacity by increasing the ratio energy-to-weight and energy-to-volume. In addition the battery has to be safe and as resistant as possible to the working environment. Hence, the battery-pack design has to take into consideration the thermal and safety issues that are linked with the technology of the adopted cells.

3.3.1 Battery technologies

The most widespread battery technologies to power electric motors in vehicles are NiMH and Li-ion. The first one was often adopted in hybrid vehicles and the second one is nowadays the standard solution for a pure EV. Table 1 shows the battery technologies adopted by some companies for certain vehicle models.

Company	Country	Vehicle model	Battery technology
GM	USA	Chevy-Volt	Li-ion
		Saturn Vue Hybrid	NiMH
Ford	USA	Escape, Fusion, MKZ HEV	NiMH
		Escape PHEV	Li-ion
Toyota	Japan	Prius, Lexus	NiMH
Honda	Japan	Civic, Insight	NiMH
Hyundai	South Korea	Sonata	Lithium polymer
Chrysler	USA	Chrysler 200C EV	Li-ion
BMW	Germany	X6	NiMH
		Mini E (2012)	Li-ion
BYD	China	E6	Li-ion
Daimler Benz	Germany	ML450, S400	NiMH
		Smart EV (2010)	Li-ion
Mitsubishi	Japan	iMiEV (2010)	Li-ion
Nissan	Japan	Altima	NiMH
		Leaf EV (2010)	Li-ion
Tesla	USA	Roadster (2009)	Li-ion
Think	Norway	Think EV	Li-ion, Sodium/Metal Chloride

TABLE 1: BATTERY TECHNOLOGIES ADOPTED BY SELECTED COMPANIES, SOURCE: SOARES ET AL. (2013), P. 16

Li-ion batteries offer higher energy density compared to NiMH. They can reach values up to 220 Wh/kg against 75 Wh/kg of NiMH. Drawbacks of Li-ion are safety issues, low and high temperature performances, which require a proper thermal management system and safety measures to protect the battery pack in case of crash. There exists a large number of different Li-ion batteries. Figure 14 shows the most common ones together with the description of their mass fraction (the ratio between the mass of each substance on the total mass of the cell). The research on batteries has been focusing on Li-ion, and an upcoming new class of advanced Li-ion may be the new generation of batteries. Some of the most capable batteries are based on Li–sulphur and Li–oxygen. The Li-sulphur current technology has a theoretical energy density range from 300 to around 600 Wh/kg, however, its practical implementation is still not possible due to problems like the shuttle effect. The shuttle effect is the formation of a highly soluble intermediate polysulfide species, which leads to a capacity fading upon cycling. The research on Li-oxygen is still at an early stage, its estimated power density ranges

from 500 to around 900 Wh/kg according to Yoo et al. (2017). Figure 13 shows the expected trend of Li-ion batteries. The diagram dates back to 2011 and its forecast for the so called "Future Li-ion" coincides with the power density available nowadays. [45] [46] [47] [48]

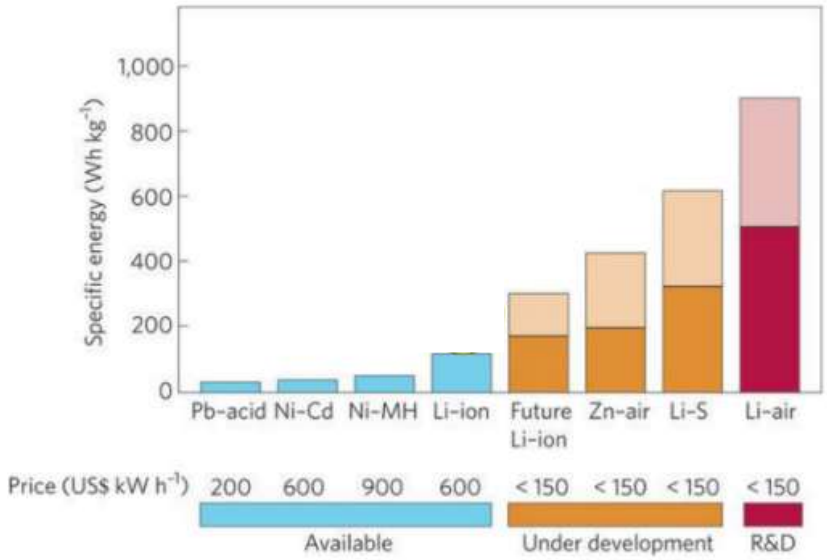

FIGURE 13: SPECIFIC ENERGIES OF SOME RECHARGEABLE BATTERIES IN 2011, BASED ON YOO ET AL. (2017), P. 1749

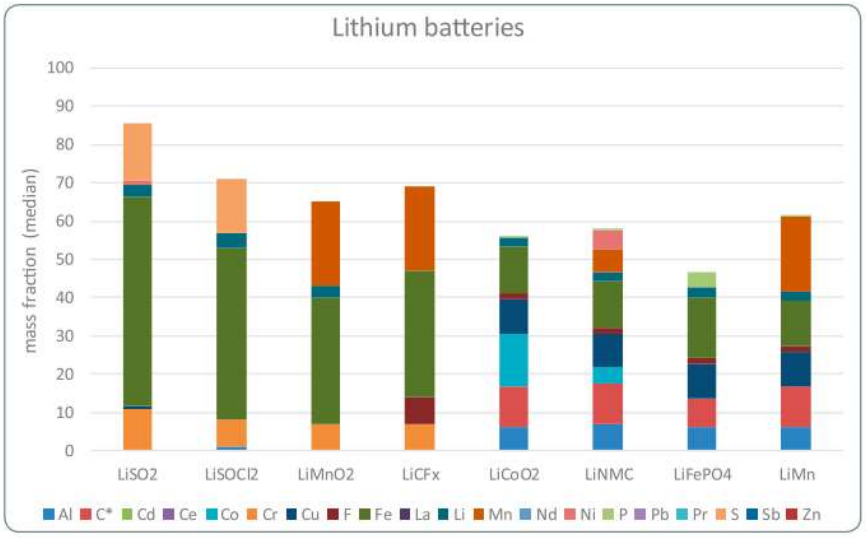

FIGURE 14: COMPOSITION OF TYPICAL LI-ION BATTERIES, SOURCE: HUISMAN ET AL. (2017), P. 21

[45] Conf. Shena et al. (2018), p. 161.
[46] Conf. Bandhauer; Garimella; Fuller (2011), p. R4.
[47] Conf. Wang et al. (2014), p. 21225
[48] Conf. Yoo et al. (2017) p. 1748-1749.

3.3.2 Heat generation in batteries

The production of heat in a battery has two origins: Joule heating and electrochemical reactions. The equation (3.8) shows the simplified version of Bernardi et al. (1985), on how to calculate the rate of heat generation in a cell. The first term is the Joule contribution and the second originates from the entropy changes. V is the cell potential (volt), I is the cell current (ampere), U is the theoretical open circuit potential at the average composition relative to a reference electrode of a given kind (volt), T is the absolute temperature (kelvin).[49] [50]

$$q_P = I * (U - V) - I * \left(T * \frac{dU}{dT}\right) \tag{3.8}$$

Quoting Onda et al. (2006) for the next three paragraphs, the heat transfer balance focused on one cell can be written as an equation (3.9). [51]

The first term is the heat rate in the cell where m is the mass of the cell, c_{cell} the specific heat, ΔT the temperature difference. The second term (q_P) is the power loss due to over potential (the Joule effect, which has already been explained above for equation ((3.8)), the third term (Q_S) is the rate of heat generated by entropy change, the fourth term (Q_B) is the heat transferred to the environment.

$$m * c_{cell} * \frac{dT}{dt} = q_P + q_S - q_u \tag{3.9}$$

The rate of heat generated by entropy change can be calculated as shown in equation ((3.10), where ΔS is the change of entropy, I the charge/discharge current, Fa the Faraday constant, n the charge number pertaining to the reaction (n = 1 for a Li-ion battery).

$$q_s = T_{cell} * \Delta S * \frac{I}{n * Fa} \tag{3.10}$$

The heat transferred to the environment due to convection and/or conduction can be calculated as in equation (3.11), where A is the total area of heat exchange and h summarises the coefficient of conduction and convection for the specific application.

$$q_u = A * h * (T_{cell} - T_{env}) \tag{3.11}$$

[49] Conf. Ismail et al. (2014), p. 2.
[50] Conf. Bernardi; Pawlikowski; Newman (1985), p. 5-12.
[51] Conf. Onda et al. (2006), p. 536.

3.3.3 Thermal runaway

Temperature plays a role in affecting life time of a battery pack, capacity and power fade, thermal runaway, electrical imbalance among cells.

As a consequence of the large number of the possible combinations of electrodes and electrolytes, a coherent analysis of all the fade mechanisms is hard to develop. In attachment 9.2 selected studies of capacity fade for several Li-ion technology are shown with specific cycle rates, number of cycles, temperature and DOD range (Depth of Discharge). For example, the study undertaken by Takei et al. shows that the capacity fade increases in proportion to the maximum cell voltage. According to the study of Choi and Lim, incrementing the DOD does not influence significantly the fade of capacity. On the other hand, the study of Belt et al. shows a strong correlation between the DOD and the power fade. In attachment 9.3, similar studies are reported on the theme capacity and power fade for batteries stored (not cycled). According to the study of Thomas et al., batteries stocked at higher SOC (State of Charge) and higher temperature have an increased power fade. Moreover, the study shows how power fade depends primarily on temperature in the first weeks, and afterwards on both temperature and time. [52]

Another phenomenon to take into consideration while designing the thermal management system of the battery pack is the thermal runaway. Part of the heat generated by the ohm effect induces an exothermic reaction which leads to an increase of reaction rate as illustrated in figure 15.

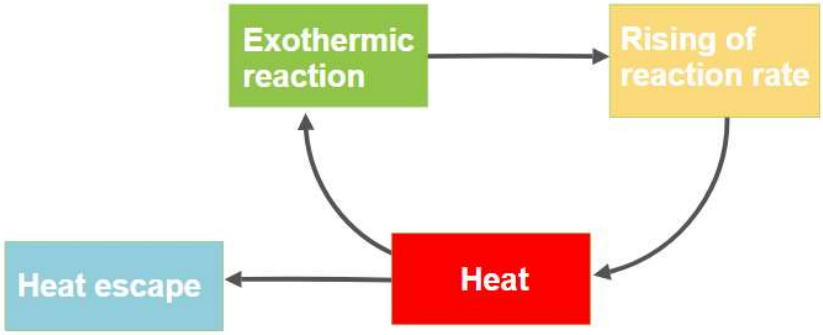

FIGURE 15: THERMAL RUNAWAY MECHANISM, SOURCE: OWN ILLUSTRATION

[52] Conf. Bandhauer; Garimella; Fuller (2011), p. R3.

The solid electrolyte interphase (SEI) is a film formed on the surface of graphite electrodes. The SEI film contains both stable and metastable components. If the temperature reaches values between 90°C and 120°C, the metastable phase is subject to an exothermic decomposition. In case the SEI is not complete, the negative electrode starts to react with the electrolyte, which is a solution of inorganic salt and organic solvent producing a reaction which can generate a temperature peak of around 200°C. Common solvents in the electrolyte solutions are ethylene carbonate (EC), propylene carbonate (PC), dimethyl carbonate (DMC), and diethyl carbonate (DEC). Whereas Lithiumhexafluorophosphate ($LiPF_6$) is the most common inorganic salt used in lithium ion batteries.[53] [54]

According to the study of Yang et al. the runaway in batteries based on Li-ion technology follows a specific path. The SEI on the graphite negative electrode starts to decompose reacting with the electrolyte when the temperature is around 85°C, in case the exothermic generation heats up to more than 110°C, a secondary film is formed and subsequently decomposed. A further increase of temperature can cause evaporation of the electrolyte (at around 140°C) or melting the separator (with temperatures ranging from 130°C to 190°C). Common electrolytes used in Li-ion batteries are likely to produce a combustion reaction if oxygen is available. For example, in cathodes made by $LiNi_{0.8}Co_{0.15}Al_{0.05}O_2$, which is a common material for cathodes, at around 225°C oxygen can be released, and the interaction with vaporized organic electrolytes can cause combustion. [55]

Figure 16 provides a comparison between two thermal behaviours of $Li_{0.5}CoO_2$ and a heating ratio of 0.2°C/min. The curve (1) shows the heat flow generated by a charged positive electrode made by $Li_{0.5}CoO_2$ in argon atmosphere. The curve (2) shows the heat flow generated in case an electrolyte ($LiPF_6$) is added to the reaction. The instability caused by the exothermic reactions is analysed by incrementing the temperature of the specimen with a rate of 0.2°C/min. It can be noticed that before reaching 130°C both samples are stable. After that, the electrode in curve (1) becomes instable once the temperature exceeds 170°C and reaches the peak of heat at around 260°C. An introduction of the above mentioned electrolyte decreases drastically the stability and introduces several exothermal reactions which can be associated to the peaks. The above mentioned compound of the electrode releases oxygen in case of temperatures exceeding 200°C according to the equation (3.12). [56]

$$Li_{0.5}CoO_2 \rightarrow \frac{1}{2}LiCoO_2 + \frac{1}{6}Co_3O_4 + \frac{1}{6}O_2 \qquad (3.12)$$

[53] Conf. Hewson; Domino (2015), p. 4-6.
[54] Conf. Wang; Sun; Chu (2015), p. 376-378.
[55] Conf. Bandhauer; Garimella; Fuller (2011), p. R4.
[56] Conf. Wang; Sun; Chu (2015), p. 376-377.

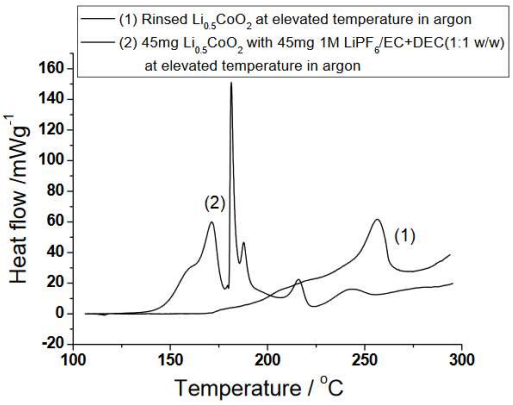

FIGURE 16: BEHAVIOUR OF $Li_{0.5}CoO_2$ WITH HEATING RATE 0.2°C/MIN, SOURCE WANG ET AL. (2015), P. 377

The charged negative electrode undergoes exothermic reactions and release of oxygen due to the decomposition of the sub-stable layer, e.g. $(CH_2OCO_2Li)_2$, of the SEI. [57]

The most common compounds to manufacture anodes nowadays are based on carbon (primarily graphite) or LTO (lithium titanate). Usually electrodes with low potential intercalation are adopted, which is defined as the reversible inclusion by the mean of energy of ions or molecules into the host materials through expanding the van der Waals gap between the sheets of the host material. In fact, this peculiarity of the electrode reduces dendrite formation. Consequently, the performances related to cycling and safety issues are improved.[58] [59]

Figure 17 shows the heat generation in a tested charged anode at high temperature. The study is based on testing in an argon atmosphere an electrode made of $Li_{0.86}C_6$ in contact with the same electrolyte solution of the previously seen test. The curve shows that there are four peaks of heat generated due to exothermic reactions. According to the author of the study, the second peak is thought to be during the decomposition of the unstable layer, e.g. $(CH_2O_2CO_2Li)_2$, of the SEI. This reaction is activated once 74°C are reached and it can release oxygen as shown in equation (3.13), hence a combustion reaction is possible. [60]

$$(CH_2OCO_2Li)_2 \rightarrow Li_2CO_3 + C_2H_4 + CO_2 + \frac{1}{2}O_2 \qquad (3.13)$$

[57] Conf. Wang; Sun; Chu (2015), p. 378.
[58] Conf. Kam; Doeff (2012), online source [accessed on 23 November 2018].
[59] Conf. Whittingha (1982), p. 229-230.
[60] Conf. Wang; Sun; Chu (2015), p. 378.

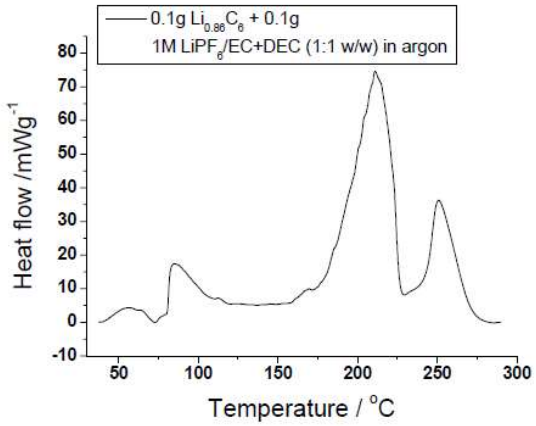

FIGURE 17: THE THERMAL BEHAVIOUR OF $LI_{0.86}C_6$ WITH ELECTROLYTE AT ELEVATED TEMPERATURE WITH HEATING RATE OF 0.2°C, SOURCE WANG ET AL. (2015), P. 378

A combustion requires oxygen, fuel and an ignition source. The battery is a closed system, so while the temperature increases and reactions generate gases, the inner pressure increases. Oxygen can be produced as seen before or it can be provided by the atmosphere, while the evaporation of electrolytes can play the role of fuel. The cooling management system has to be designed in order to guarantee temperature below around 66°C (in case of negative electrodes based on Lithium Carbon), and a safety range is required, in order to avoid reactions of runaway which quickly rump up the temperature with the risk of a no return point by generating a chain of exothermic reactions. The phenomenon of temperature of no return can be described with the graph shown in figure 18. The graph describes the generation of heat compared to the thermal dissipation. Thermal dissipation depends on the cooling system and the environmental temperature. The heat produced by the reactions is displayed in the form of an exponential curve according to the Arrhenius law (equation 33.14). The three lines (1, 2, 3) represent different coolant performances starting at three different temperatures (A, B, C) to interact with the heat generation. In line 3, the coolant is not able at any point to absorb enough heat generated by the reaction. Whereas, in case the coolant behaves as represented in line 2, there is a point at which the cooling system removes all the produced heat. This point (D) is called critical because above it the thermal runaway is ignited. Line 1 has two points of intersection with the heating curve and both of these points describe isothermal operations. Point E is called stable, since the removing heat power of the cooling system is sufficient even if the temperature rises. The cooling system is able to remove all the produced heat till point F included, which represents a critical point. In fact, after point F the reaction generates heat faster than the coolant can absorb it, and hence, the thermal runaway is ignited. An unstable point is also named “Temperature of non-return”.[61]

[61] Conf. Wang; Sun; Chu (2015), p. 377-382.

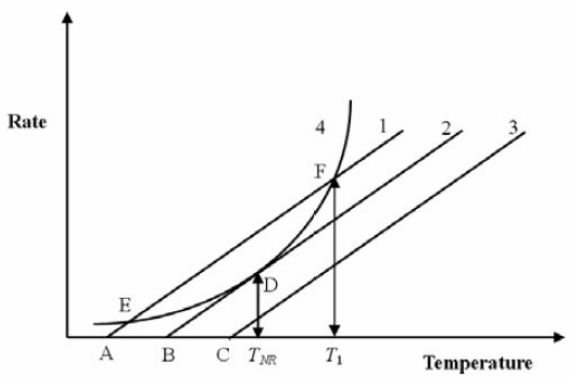

FIGURE 18: THERMAL RUNAWAY, SOURCE WANG ET AL. (2015), P. 379

$$k_{heat} = k_0 * e^{-E/RT} \tag{3.14}$$

The Arrhenius law is shown in equation 3.14, where k describes the rate of the reaction at the temperature T, k_0 is the frequency factor for a particular reaction, E is the activation energy (in the same unit as $R * T$) and R is the universal gas constant.[62]

$$\frac{dT}{dt} = -k_{cool}(T - T_a) \tag{3.15}$$

Equation 3.15 shows the Newton law in the case of cooling. The first term on the left of the equation is the rate of change of temperature on time, k is the heat exchange coefficient, T is the temperature of the system and T_a is the temperature of the surroundings.[63]

One trigger of the thermal runaway is that the reactions, which generate heat in a battery, make less resistive to current passage the heated area. Less resistance, leads to an increase of current flow, which generates more heat, more heat reduces further the resistance. Thus, the central regions, the ones further away from the coolant, are the ones more affected by this phenomenon.[64]

[62] Conf. Hall (1999), p. 18.
[63] Conf. Cheng et al. (1999), p. 4.
[64] Conf. Verbrugge (1995), p. 1558.

3.3.4 Battery-pack heating

The internal resistance of a battery at low temperature increases, lowering the maximum voltage. Applying a higher voltage could damage the battery, hence the charging process has to be slowed down. The same is true when discharging the battery at temperatures which are under the optimum thermal range, which for Li-ion (in specific the $LiFePO_4$ 5Ah 3.2V) is considered to be between 10-40°C according to Sun et al. (2014). Sun et al. tested the previously mentioned battery at different temperatures and registered that the capacity changes as shown in figure 19 (a). The change in the ohmic resistance is also observed at different SOCs (State of Charges) and different temperatures. The battery has to be replaced if the capacity reaches 80% of the initial one and if this value is reached at approximately 0°C and if at -20°C it has lost almost all the capacity. [65]

Cycling the Li-ion cell at low temperature causes irreversible damages as shown by Matadi et al. (2017). In their experiment the 16 Ah C/NMC Li-ion cells were cycled between 4.2V and 2.7V (100% to 0% of SOC with 1C (1C stands for one discharge cycle in one hour) and after 50 cycles at 5°C the loss of capacity was on average 75%. According to the authors the same cell can be cycled at 45°C for 4000 cycles before reaching a critical capacity fading. [66]

This analysis clarifies that a heating of the battery pack has to be designed in order to warm up the battery before charging or using it to power the vehicle. This can be done with a dedicated resistance heating or with the one of the cabin cooling. The first option can achieve better performances (like shorter warming up time) since the system is designed on purpose for the battery pack, the second may reduce the manufacturing costs.

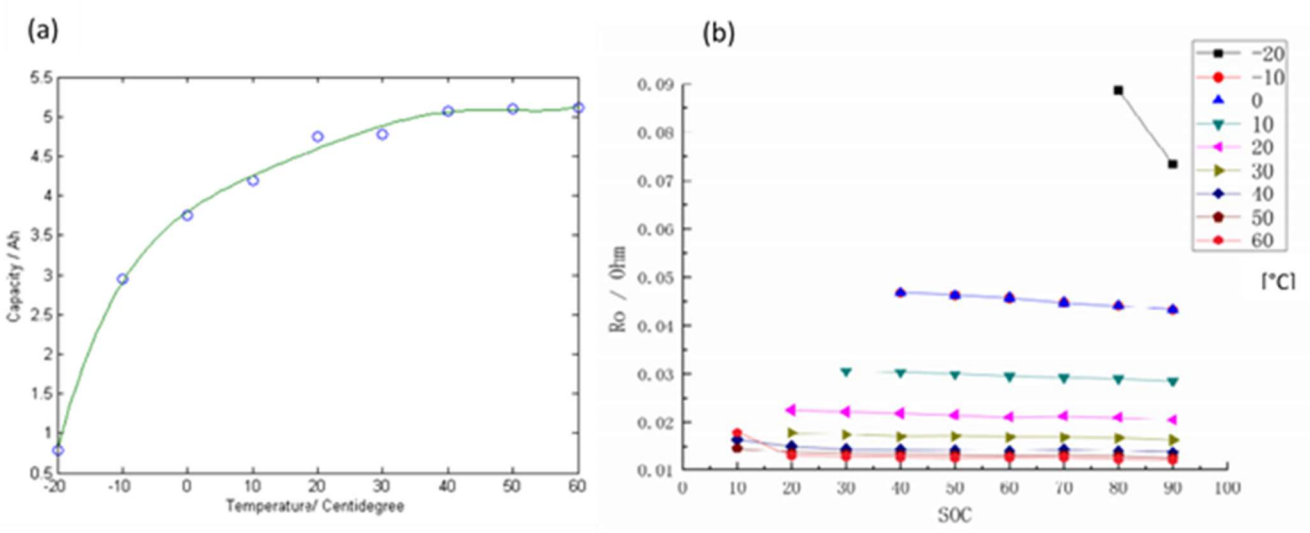

FIGURE 19: VARIATION OF THE CAPACITY AT DIFFERENT TEMPERATURES (A), VARIATION OF THE INTERNAL RESISTANCE AT DIFFERENT SOCS AND TEMPERATURES (B), BASED ON SUN ET AL. (2014), P. 480

[65] Conf. Sun et al. (2014), p. 476-483.
[66] Conf. Matadi et al. (2017), p. 2374-2388.

3.3.5 Battery-pack cooling systems

Once the critical temperatures for the selected battery technology are known, the cooling system can be designed. The design of the battery pack cooling system includes the selection of the form of the cells, how they are stacked together, how the coolant interacts with the stacks and how the stacks are arranged in the pack which is mostly determined by the position of the pack in the body of the vehicle.

The cells are usually made of aluminium and the choice of the geometry is mainly between three options: cylindrical, prismatic and pouch. The first two options foresee that the active material is packed in coils and then stored in the cell case, whereas the third option foresees that the layers of active material are stacked. The different geometries can be analysed from the cooling performances point of view by defining the ratio surface to volume. In fact, a high value of this ratio stands for a better possibility to remove heat from the cell. The worst ratio of the three geometries is the one of the cylindrical cell. As a matter of fact, considerable heat generation on the radial dimension can occur. In addition, the curved outer surfaces of this cell are particular challenging to be fitted with cooling systems. Despite its poor cooling performance, the cylindrical cell is one of the most adopted. The reason is the good trade-off offered between the other parameters, such as costs, availability, and safety. In fact, cylindrical cells are easier to manufacture and have good mechanical stability since their geometry can resist to high internal pressure without any deformation. The process of packing the material inside a cylindrical case requires less time than in case one of the other two geometries is used. In cylindrical cells the foils of the electrodes and the two separating foils are rolled up by a circular section and then inserted. In prismatic and pouch cells, the foils can be cut and laid flat, "Z" can either be folded or rolled up.[67] [68]

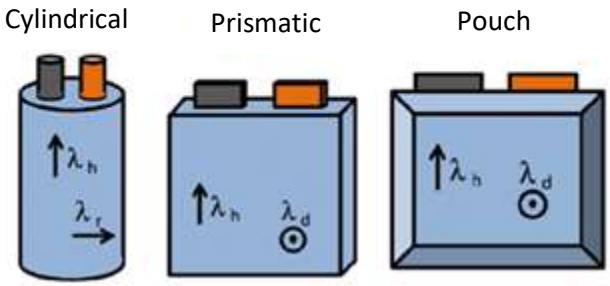

FIGURE 20: CELL GEOMETRIES, BASED ON WIEBELT ET AL. (2009), P. 13

A benchmark conducted by Erriquez et al. (2017) and published by McKinsey investigated the energy density of ten of the most produced EVs and compared the energy density with the geometry. The highest energy density of the cylindrical cells can be 25% higher than the one of the pouch cells and even 53% higher than the one of the prismatic cells. The cylindrical cells are able to provide an energy density 25% greater than the pouch cells and 53% greater than the prismatic ones (cylindrical cells 245 Wh/kg, pouch cells 195 Wh/kg and prismatic cells 160 Wh/kg). In case of liquid cooling the cylindrical cells are more challenging to cool and the system of pipes for these cells is generally heavier than for the other two types of cells. The differences are further analysed on the following pages of this chapter.[69]

[67] Conf. Wiebelt et al. (2009), p. 13-15.
[68] Conf. Oak Ridge National Laboratory (2013), online source [accessed on 23 November 2018].
[69] Conf. Erriquez et al. (2017), online source [accessed on 23 November 2018].

Regarding the geometry of the battery pack, common solutions for battery pack geometries of BEVs are the so called T-shape and the Mat-shape. The first one implies setting the batteries in a coaxial direction with the central tunnel and with the space available under the seat panel. This configuration offers good protection from front and rear crash, but problems arise as far as side crash safety is concerned. The latter is usually referred to an architecture which describes a battery pack arranged on the entire floor area of the cabin. Compared to the T-shape it may host more battery cells and keep the gravity point lower. As for the T-shape, side crash represents an issue of high relevance in order to guarantee the integrity of the battery. In both cases the battery pack design has to be accommodated with a view on the ergonomics.[70]

FIGURE 21: T-SHAPE OF THE BATTERY PACK IN THE CHEVROLET VOLT (2012) ON THE LEFT, MAT-SHAPE IN THE NISSAN LEAF (2013) ON THE RIGHT, ARCUS (2016), ONLINE SOURCE [ACCESSED ON 25 NOVEMBER 2018]

The heat removal from the cell has to be designed by choosing the coolant and the transfer mechanisms (conduction, convection). The choice of coolant is usually between an air and a water solution with antifreeze (like ethylene glycol).

Air cooling has advantages over liquid cooling, such as lower price, greater reliability and the fact that the design of the channels is easier since the interface with the cell is less complex. Some disadvantages compared with liquid cooling are a low heat removal rate and the poor homogeneity of the flow.

Air battery thermal management can be divided in passive and active. The passive one describes a system in which the inlet air is taken from the environment without pre-cooling or pre-heating, the active management uses a HVAC (Heating Ventilation and Air Conditioning) system to change the temperature of the inlet air.

Forced air cooling in a battery pack was investigated by Lu et al. (2015). Their study consisted in varying the number of air inlets (15, 17 and 52 air inlets) of a battery pack with high density of Li-ion battery: 252 Li-ion batteries (type 32650) in 0.021m^3. The desired range of temperatures was set between 20°C and 40°C. The study showed how it is possible to cool the batteries for low and medium heat generation (4.375 W/m^{-2} and 8.75 W/m^{-2}) by increasing the number of inlets and the speed of the air whereas for high heat generation (16.5 W/m^{-2}) it is required to decrease the inlet air temperature.[71]

[70] Conf. Khajepour; Fallah; Goodarzi (2014), p. 110-114.
[71] Conf. Lu et al. (2015), p. 2-8.

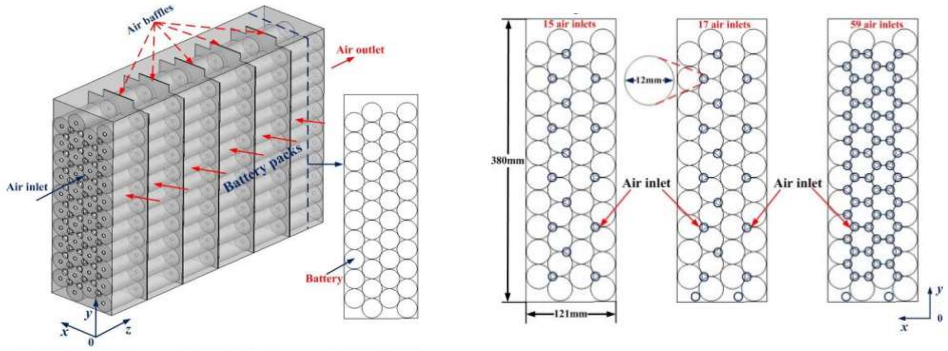

FIGURE 22: MODEL OF FORCED AIR COOLING WITH DIFFERENT AIR INLETS, SOURCE LU ET AL. (2015), P. 2

To decrease the inlet temperature two solutions are possible. The first one is to provide an AC system dedicated for the battery pack, the second one is to use the same one as for the cabin. The latter is implemented for example in the 2018 Nissan e-NV200 with a battery pack power of 40 kWh. The same system is implemented in the 2014 version that is provided with a 24 kWh battery pack power. The air coming from the HVAC is directed to the battery pack to guarantee the optimal range of temperatures for the functioning of the cells. Nissan designed it to work during the quick charging mode, when the generated heat is potentially high; heating is used in case the temperature is too low.[72] [73]

Systems which are using fluid coolant to remove heat from the battery pack offer higher heat removal performances and are usually more compact since the coolant flow required is reduced.

Two approaches are possible: to immerse the cells in the coolant or to provide the battery pack with pipes in which the cooling fluid flows; by being in contact with the cells the heat is transferred to the fluid.

Immersing the cell in a coolant is an expensive and complex solution, although it is highly efficient. This solution is for example adopted by the Taipei-based XING Mobility company for their supercar Miss R. The battery pack is composed by 4200 Li-ion batteries (type 18650) divided into 42 liquid cooled modules. The fluid has to be a dielectric fluid with high heat transfer capacity. Dielectric fluids have extremely low conductivity and therefore they are often applied where electrical isolation is required. The above mentioned car uses the 3M Novec 7200 Engineered Fluid.[74]

The cooling solution with pipes usually adopts a water solution of ethylene glycol to avoid ice formation. Different types of cooling setups can be implemented. According to the cell dimensions, bottom-, top-, or side-cooling are possible. The first one is adopted when the height dimensions of the cell are moderate, and when the cooling pipes can remove the exceeding heat by being in contact with the bottom or the top of the cell. The arrangement of bottom cooling has the advantage that in case of leakage the probability of coolant flowing in the battery pack is minimised. In case the above mentioned contact is not sufficient because the evacuation of the heat flux requires a lateral cooling, other solutions are possible. For example, it is possible to provide fins on the sidewall of the cell. The fins are made of conductive materials and lead the heat to a cold plate in contact with the coolant

[72] Conf. Romain (2014), online source [accessed on 25.11.2018].
[73] Conf. Nissan (2018), online source [accessed on 25.11.2018].
[74] Conf. Blain (2017), online source [accessed on 25.11.2018].

flow. This is efficient in prismatic and pouch cell geometries. An example of this cooling architecture can be seen in the 2017 Chevrolet Bolt EV. In its battery pack, between each two cells a conductive material acts like a fin leading the heat to a plate on the bottom. The plate is manufactured in order to receive coolant on one side. It leads it through the frame with an optimised path to remove the required heat and lets it flow away in a second channel, opposite to the income flow. A pump assures that the coolant flows into a heat exchanger and then back to the battery pack.[75]

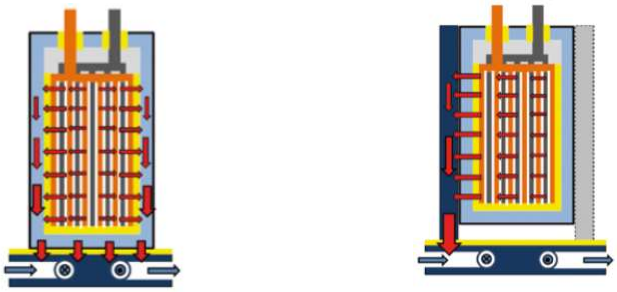

FIGURE 23: HEAT FLUX WITH BOTTOM COOLING (ON THE LEFT) AND WITH THE AID OF LATERAL FINS (ON THE RIGHT), SOURCE WIEBELT ET AL. (2009), P. 14

[75] Conf. Wiebelt et al. (2009), p. 14.

Tesla owns a patent (patent number US20110212356A1) on a lateral cooling system, which is adopted in the Model S, Model X and Model 3. In all these three models the Li-ion cells are cylindrical, model 18650 for Tesla S and X and model 2170 for Tesla 3, which is, according to J. B. Straubel (CTO of Tesla), around 47% bigger and from 10 to 15 % more energy efficient than the 18650 cell[76].

The cooling system has also been changing, the first concept that is adopted in the Model S85 was a cooling tube interacting with the lateral surface of the cylindrical cells. One tube for one module (444 cells). A second architecture was developed for the model P100, in which two tubes are assigned to each module of the battery, hence each tube cools 258 cells. A next generation of cooling architecture appeared on Tesla 3. While for the previous two the cooling system is definable as in series, this architecture adopts a parallel configuration, letting the coolant flowing every two rows of cells in and merging the flows before the outlet. In this configuration each pipe is responsible for approximately 164 cells.[77]

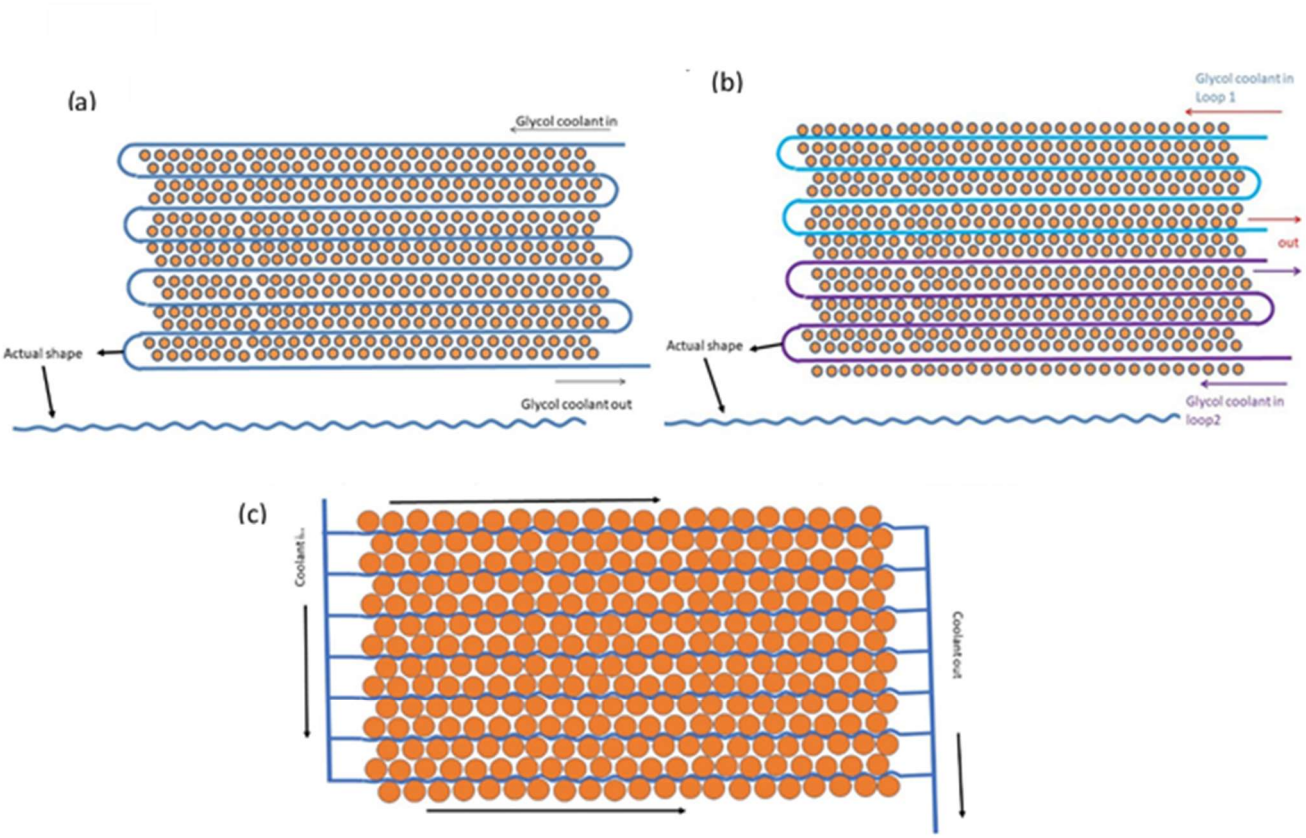

FIGURE 24: TESLA´S FIRST (A), SECOND (B) AND THIRD (C) COOLING ARCHITECTURE, BASED ON BOWER (2018), ONLINE SOURCE [ACCESSED ON 25 NOVEMBER 2018]

[76] Conf. Hawley (2017), online source [accessed on 25.11.2018].
[77] Conf. Bower (2018), online source [accessed on 25.11.2018].

3.3.6 Comparison of cooling strategies

Dafen Chen et al. (2016) compared different cooling systems for a prismatic Lithium-ion cell of 35 Ah, measuring 169mm in width, 179mm in length, and 14mm in thickness. The electrodes are made of graphite (the anode) and a mixture of NMC and MnO (the cathode). The tests were conducted by removing the heat from the two widest lateral surfaces. Four different configurations are studied: air cooling, direct liquid cooling, indirect cooling and fin cooling. In the analysis of Dafen Chen et al. direct cooling is done by immersing the battery cells in a dielectric fluid. However, OEMs usually do not adopt direct cooling for several reasons, such as the high risk of leakage, increase of complexity, thermal inhomogeneity in the flow. By keeping the same average as a goal for the cooling system, it was shown as the air cooling needs between twice and three times more energy, fin cooling increases the weight of the cell of around 40%, indirect cooling has the highest maximum temperature difference (inlet - outlet) due to the longest coolant path. Direct cooling scores the highest cooling performances with a good uniform temperature distribution, followed by indirect cooling. [78]

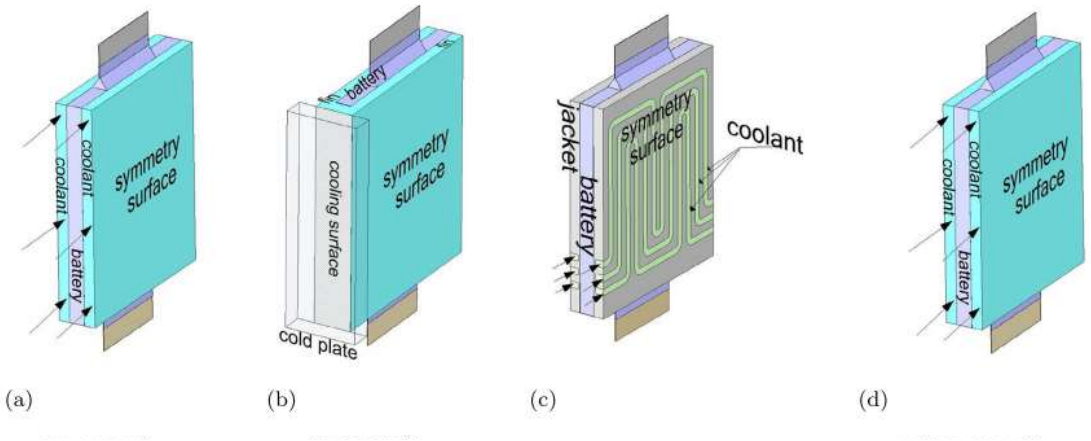

FIGURE 25: THE FOUR CONFIGURATIONS TESTED: AIR COOLING, FIN COOLING, INDIRECT LIQUID COOLING AND DIRECT LIQUID COOLING, BASED ON CHEN ET AL. (2016), P. 849

[78] Conf. Chen et al. (2016), p. 846-854

3.3.7 Tab cooling

A further possible cooling method is the tab cooling. Tab cooling represents a complex solution. In fact the tabs need to be in contact with conductor elements on whose surface the coolant flows while the insulation between the cells and the coolant has to be guaranteed. At the time of writing, no case is known in which tab cooling of a battery pack of an EV has been applied. The study of Hunt et al. (2016) tests surface cooling systems compared to tab cooling. Both air and liquid cooling are compared, although air cooling is neglected in the following comparison since its cooling performances are substantially lower. The cooling goal was set at 20°C for the surface and for the tab according to the system tested. The experiment consists in cycle 5Ah Kokam pouch cells at different rates between 4.2V and 2.7V and with the above mentioned cooling systems, capacity and power fade as well as impedance were measured every 50 cycles. The discharging rate is measurable by the number of cell discharges in one hour. In the experiment, at low discharging rates, like C/20, no appreciable difference between the cooling systems were measured. However, at the rate of 6C, the surface cooling battery lost approximately three times more useable capacity compared to the tab cooled after 1000 cycles: 3.84Ah versus 4.61Ah. According to the authors of this test, this difference can be explained by two reasons: the first reason is that the tab cooling leads the different layers of the pouch cell to be at almost the same temperature, whereas surface cooling does not and hence no uniform impedances between the layers are produced which decreases the useable capacity of the cell. The second reason is related to the generation of currents correlated to the different temperatures between the layers. This leads to a non-uniform distribution of loss of active lithium, which leads again to a higher increase of cell impedance and power fade. According to the results of this study tab cooling could represent an extremely relevant improvement for the life of batteries in EVs. [79]

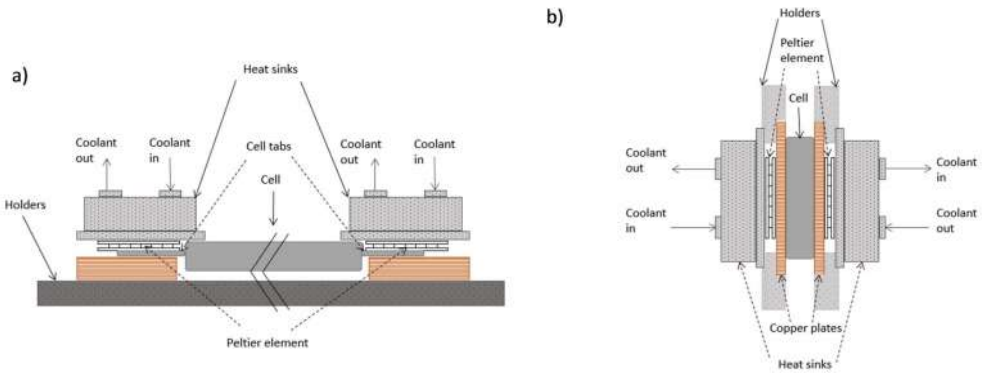

FIGURE 26: TAB COOLING (A) AND SURFACE COOLING (B) SYSTEMS, SOURCE HUNT ET AL. (2016), P. 1847

[79] Conf. Hunt et al. (2016), p. 1846-1852.

3.4 Electric motors

As mentioned in chapter 4.1, the two most frequently adopted technologies for EMs are IMs and PMMs.

An IM has two main parts: the stator and the rotor. The stator has usually three coil windings in which a three-phase AC flows. The winding system is allocated in slots of the stator. The slots are a stack of highly permeable steel laminations inside a frame. The three-phase AC current, by passing through the windings, produces a rotating magnetic field (RMF). The speed at which the magnetic field rotates is known as synchronous speed. This magnetic field induces an EMF in the rotor (which can be simplified by a closed loop of conducting material), which generates a current in the closed loop according to Faraday´s law. Hence, an electromagnetic force is produced on the loop, which will start to rotate according to the Lorentz force law. In the IM, the rotor is built as a squirrel cage. The rotating magnetic field of the stator windings induces current in the bars of the squirrel cage, which is shorted by end rings and thus, behaves like loops. The squirrel cage will then start rotating. To minimize losses due to the eddy current, insulated iron core lamina are packed inside the rotor.[80]

Copper and aluminum are possible choices for the material for the squirrel cage of an IM. A detailed list of the properties of the two materials is shown in attachment 9.1. The cage can either be constructed or die-cast. The fabrication steps are: pre-heating of the core, in which the rotor is inserted, arrangement of the bars, machining of the bars, welding (for the aluminium) or brazing (for the copper). Die casting is a process that can be highly standardised and guarantees a better uniformity of the production volume as well as shorter lead times. Die casting requires higher investments. To depreciate those costs, high production volumes are needed. As shown in the table below, compared to aluminium die casting, copper die casting requires higher temperatures and pressures.[81] [82]

	Aluminium	Copper
Melting temperature (°C)	660	1080
Equipment needed	Standard die casting	Temperature control
	No preheated dies	Preheated dies
Shot Pressure (bar)	138	450
Clamp pressure (bar)	166	538
Material cost ($/Kg)	2.13	7.4
Material density (g/cm^3)	2.7	8.7

TABLE 2: COMPARISON OF ALUMINIUM AND COPPER DIE CASTING PARAMETERS, BASED ON FINLEY, HODOWANEC (2001), P. 2 AND CONF. MECHLER (2010), P. 20

[80] Conf. Cox (2007), p. 26-32.
[81] Conf. Finley, Hodowanec (2001), p. 2.
[82] Conf. Mechler (2010), p. 20.

According to the study on EMs for mini vehicles, the efficiency of the motor adopting copper as material for the squirrel cage increases significantly (up to 5%) the efficiency of the motor. [83]

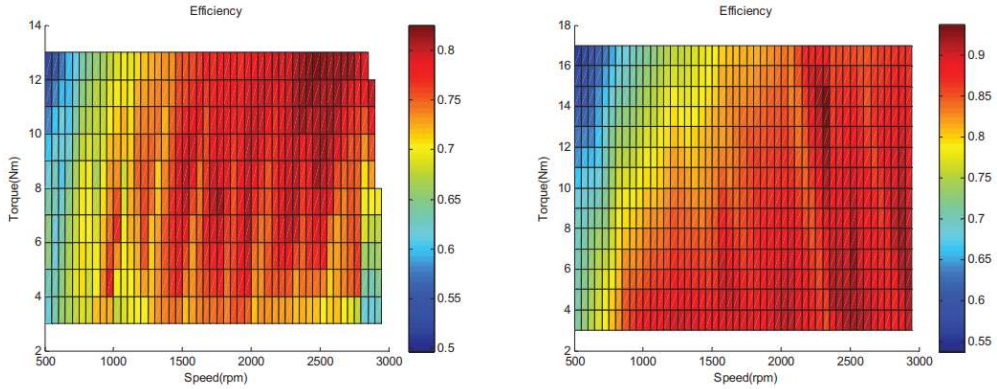

FIGURE 27: COMPARISON OF THE EFFICIENCIES OF AN IM USING COPPER (LEFT) AND ALUMINIUM (RIGHT) FOR THE SQUIRREL CAGE, SOURCE: CHENG ET AL. (2012) P. 255

A PMM is made by a rotor and stator as well, although the functional principles are different. The rotor produces a constant magnetic field and the stator an RMF. The RMF is produced in the same way described above for the IM. The rotor is provided with magnets arranged by alternating their poles. The constant magnetic field of the rotor interacts with the RMF of the stator. In PMMs the rotor needs a starter that provides an initial rotation. Thanks to it, the magnetic fields lock together and rotate at the same speed (N_s). For this reason, the PMMs can be classified as a synchronous speed motor. This speed can be accurately controlled through the number of poles (P) and the frequency (f) of the electricity as shown by equation (3.16). The starter is needed to win the initial inertia of the rotor and to boost the rotor to the synchronous speed. Once this speed is reached the starter stops to act. This inertia combined with the alternating of the magnet poles, and hence an alternating of attraction/repulsion forces between the rotor and stator, would impede the rotor to spin. [84]

$$N_s = \frac{120 * f}{P} \tag{3.16}$$

Quoting AVID Technology for the next two paragraphs, there are different possible layouts of the rotor of a PMM. In particular for EVs two types are interesting: the surface permanent magnet (SPM) and the interior permanent magnet (IPM).[85]

In the SPM, the magnets are fixed to the surface of the rotor, either held in place by a composite tape or wrapped around as a ring to the rotor. This type of EM is suitable for high speed applications and ensures high efficiency. The rotor losses are minimized since the magnets are acting directly in the air gap between stator and rotor. A disadvantage is a high ratio of torque produced on magnetic material

[83] Conf. Cheng et al. (2012), p. 256.
[84] Conf. Gieras, Wing (2002), p. 169-186.
[85] Conf. AVID Technology (2018), online source [accessed on 15.11.2018].

in comparison to other EM types. Another drawback are the higher costs connected to the retention system of the magnets.

The IPM rotor, which is manufactured by a stack of laminated steel sheets, has moulded or punched slots to house magnetic bars. Compared to an SPM rotor, the IPM has a better ratio of torque produced on magnetic material thanks to a lower reluctance. On the one hand, the mechanical location of the magnets in the slots simplifies the manufacturing process since there is no need of rating systems or banding, on the other hand it can be complex due to the fitting of the magnets in the layers of lamination steel and it requires complex automated machinery.

3.4.1.1 Cooling requirements of the different types of electric motors

The heat produced in an EM is identified as part of the losses occurring in the motor. With induction motors the losses can be stator copper losses, stator core losses, rotor bar losses and friction losses. The heat transfer takes place in three ways: conduction, convection and radiation. The type of machine, the load and the supply are the most important parameters which influence losses. The design of an appropriate cooling system leads to higher efficiency, longer lifetime and lower overall cost. [86] [87]

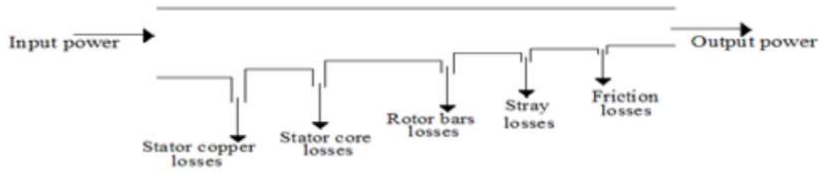

FIGURE 28: TYPES OF LOSSES IN INDUCTION MOTORS, SOURCE BADRAN ET AL. (2012), P. 77

According to Badran et al., the hottest element in an IM are the rotor bars and the stator winding. The heat in these parts is mostly generated by the copper and bar losses[88]. Quoting Bonnett, under normal running condition, the stator winding will be the limiting factor concerning the temperature in an induction motor[89].

[86] Conf. Badran; Sarhan; Alomour (2012), p. 77.
[87] Conf. Jandaud; Le Besnerais (2017), p. 39.
[88] Conf. Badran; Sarhan; Alomour (2012), p. 75.
[89] Conf. Bonnett (2001), p. 1129.

Analysing the flux generation of IMs, a difference has to be made between rotors adopting aluminium and copper as material of the rotor bars. As shown in Table 3 and attachment (9.1), aluminium has the worst thermal conductivity, a higher specific coefficient and a higher coefficient of thermal expansion, thus in equal operating conditions and motor layout, rotor bars in aluminium are hotter and expand more compared to rotor bars in copper.[90]

Material	Thermal conductivity (W/m.C)	Density (Kg/m^3)	Specific heat (J/Kg.C)
Iron	58	7850	420
Aluminum	222	2790	833
Steel	35	7770	460
copper	388	8933	385
Ambientair	0.02624	1.127	1007

TABLE 3: THERMAL PHYSICAL PROPERTIES OF THE MATERIALS IN INDUCTION MOTORS, SOURCE BADRAN ET AL. (2012), P. 82

The cooling system of PMs represents a further challenge. In fact, the rare earth materials undergo to a phenomenon called demagnetisation, which is temperature dependent. The most frequently adopted rare earth material for PMs in EVs is NDFeb (Neodymium Iron Boron). This material has better magnetic properties than other common magnetic materials. As shown in figure 29, the flux density and coercivity of NDFeB score high values. The remnant flux density is the measure of magnetisation, its SI unit is Tesla (T). Coercivity shows the ability to resist against demagnetisation once the material is magnetised. Dysprosium is often added to NdFeB to increase the high temperature coercivity to values exceeding 100°C. [91]

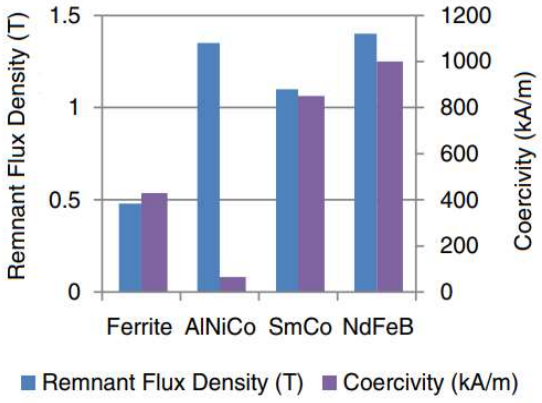

FIGURE 29: COMPARISON OF REMNANCE AND COERCIVITY FOR DIFFERENT HARD MAGNETIC MATERIALS, SOURCE WIDMER, MARTIN, KIMIABEIGI (2015), P.8

[90] Conf. Finley; Hodowanec (2001), p. 6.
[91] Conf. Widmer; Martin; Kimiabeigi (2015), p. 7-8.

As mentioned before, magnets are sensitive to temperature. The property of coercivity and flux density are in fact temperature dependent. An increase of temperature leads to a decrease of those properties as it can be observed in figure 30, in which the normal and intrinsic curves of NdFeB are shown. The consequence is that the operating performances of the motor are strongly correlated to the magnet temperatures. The loss of magnetisation can be irreversible. The graph shown in figure 30 can be used to determine it. By drawing a line with the inclination of the permeance coefficient and intersecting it

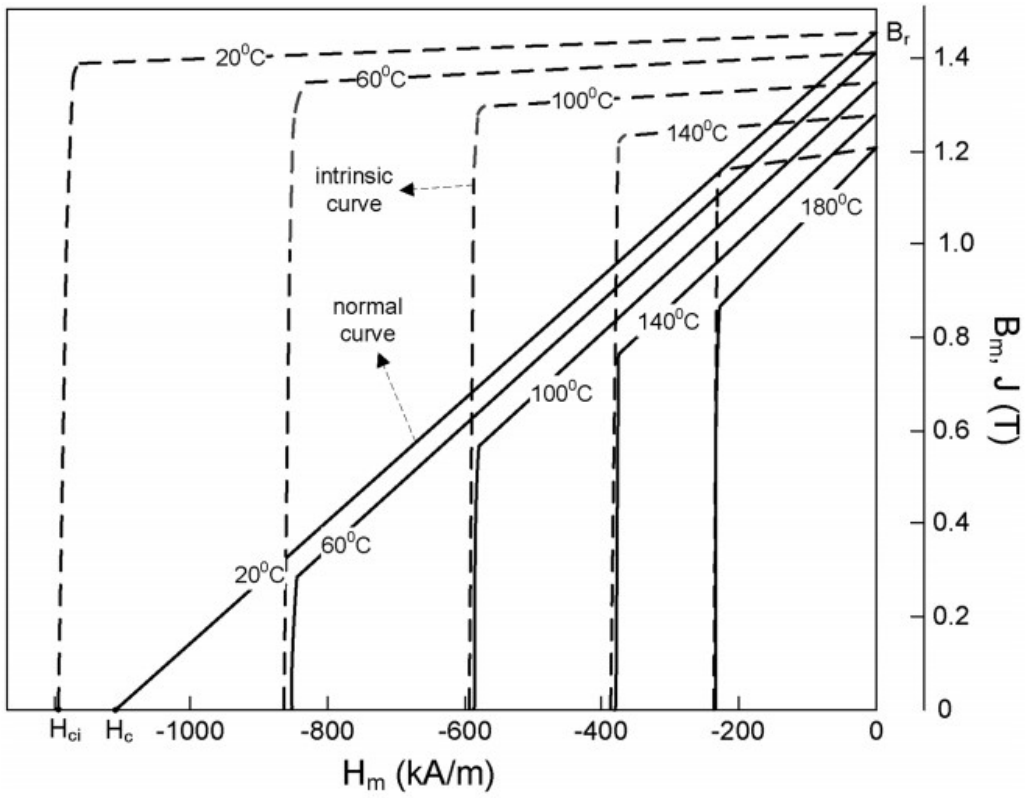

FIGURE 30: DEMAGNETISATION AND CHARACTERISTIC CURVES OF A PM (TDI NEOREC 53B IRON BASED RARE-EARTH MAGNET), SOURCE YANG ET AL. (2015), P. 3

with the normal curve of the working temperature, it is possible to understand if irreversible magnetisation happens (the intersecting point is above the knee of the normal curve) or not (the intersecting point is under the knee of the normal curve). The point at which irreversible demagnetisation happens is called Curie point. It defines the Curie temperature which has to be a fundamental parameter while designing the cooling system.[92]

[92] Conf. Yang; Schofield; Preindl (2016), p. 3-4.

As mentioned before, some of the elements which face an important increase of temperature are the windings of the stator. To prevent possible winding-to ground shortcuts, slot insulators are arranged in the stator as shown in figure 31. Typical insulations are based on aramid or BoPET layered papers. Desired properties for these systems are flexibility, chemical resistance, high dielectric breakdown strength and thermal resistance. Insulation classes are defined as shown in figure 32 and they are characterised by a maximum permissible temperature.[93]

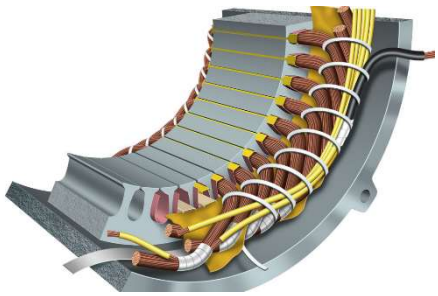

FIGURE 31: STATOR WINDING INSULATION, ONLINE SOURCE: STUDIO SAYERS, ACCESSED ON [18.11.2018]

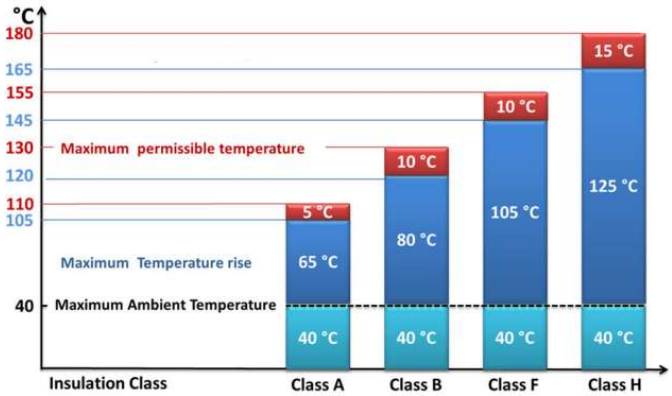

FIGURE 32: THERMAL LIMITS FOR INSULATION CLASSES, BASED ON MOHAMMED, DJUROVIC (2018), P. 2

[93] Conf. Yang; Schofield; Preindl (2016), p. 107.

3.4.1.2 Cooling strategies

The traditional motor cooling consisted of self-ventilated motors, possibly accompanied by an integrated fan. In self-ventilated motors the circulation of the air is influenced by the spinning of the rotor, air circuits channel the air towards the outside of the motor housing. The design of the air circuits can be radial, axial or a mixture of both architectures. Fins are on the motor cage to improve the dissipation of the heat. [94]

Self-ventilated motors can be adopted for low power density machines, such as certain hybrid vehicles in which the electrical contribution to the propulsion is low. The advantages are low costs and simplicity of the layout.

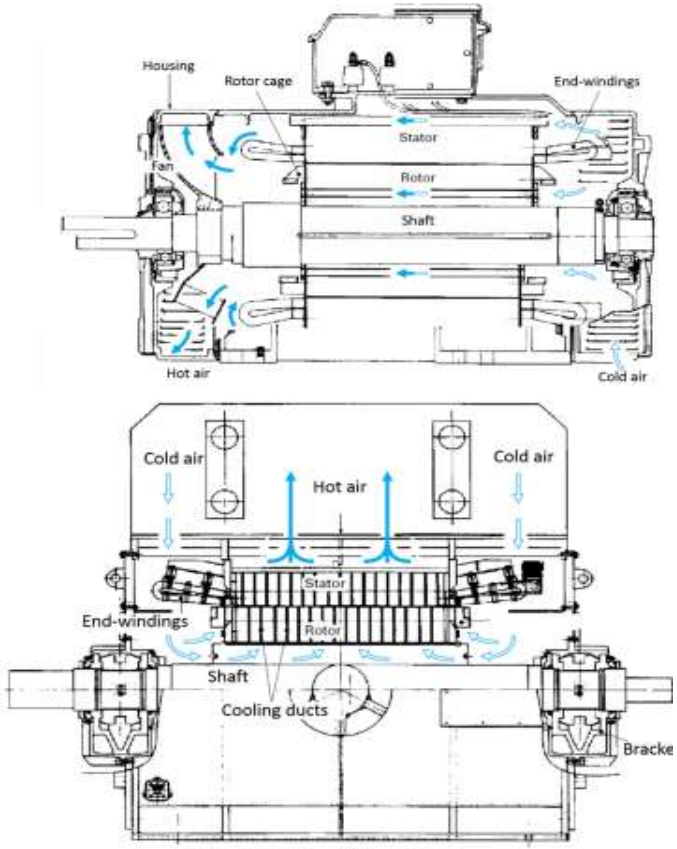

FIGURE 33: AXIAL (UPPER) AND RADIAL (LOWER) COOLING CIRCUIT ARCHITECTURE, SOURCE JANDAUD AND LE BESNERAIS (2017) P. 23

[94] Conf. Jandaud; Le Besnerais (2017), p. 23.

For higher needs of heat dissipation, one or more fans can be integrated. Although it is possible to design a fan powered separately, fans are usually mounted on the rotor axle and are bi-directional in order to work during regenerative braking as well. The materials they are made of are hard polymers, aluminium or steel. The final choice is a trade-off between costs and weight optimisation.[95]

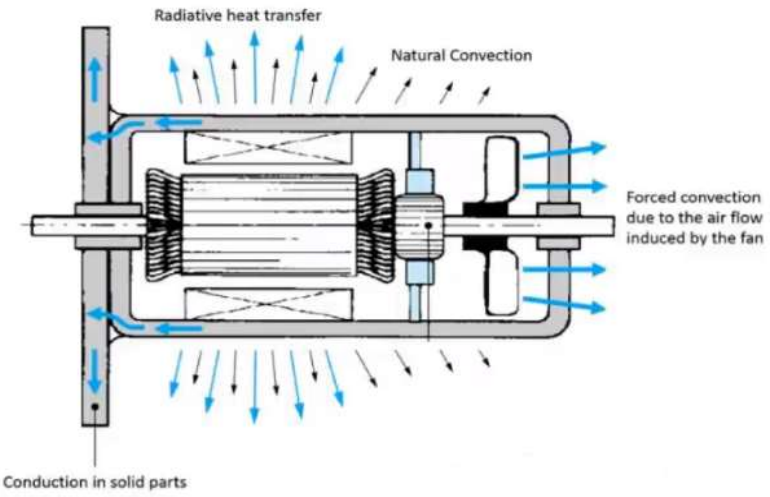

FIGURE 34: HEAT PROPAGATION WITH FAN AIR COOLING, SOURCE JANDAUD AND LE BESNERAIS (2017) P. 8

The trend of EMs in the automotive industry is towards more compact and more performant motors, hence a rise in the power density, which leads to a greater heat flux and to more challenging cooling solutions.

Liquid cooling is a solution for high power density motors, the coolant is usually water or oil. There exist tow possible topologies: with water jackets and with water ducts inside the stator. The first one can be considered part of the housing and it is less complicated to manufacture compared to the second one, which, however, has better performance in removing the heat. On the one hand they are very effective configurations, on the other hand they require a pump to force the flow in the system.[96]

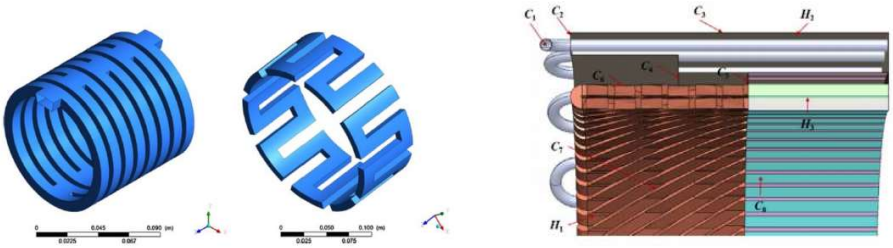

FIGURE 35: WATER JACKETS (ON THE RIGHT), AND WATER DUCTS INSIDE A STATOR (ON THE LEFT), SOURCE JANDAUD AND LE BESNERAIS (2017) P. 24

[95] Conf. Barnes (2003), p. 60.
[96] Conf. Jandaud; Le Besnerais (2017), p. 24.

The 2012 Nissan Leaf, which has a PMM, has a cooling motor system designed with water jackets. The three water jackets are implemented in the motor housing. Figure 36 shows a diagram displaying the rise of temperature in the motor of the 2012 Leaf at the increasing of the power rate. The test was done by keeping the rotational speed at 7000 rpm. The highest temperature of the motor can be measured in the stator winding where it reaches a peak of around 140°C at the maximum motor power (80kW). [97]

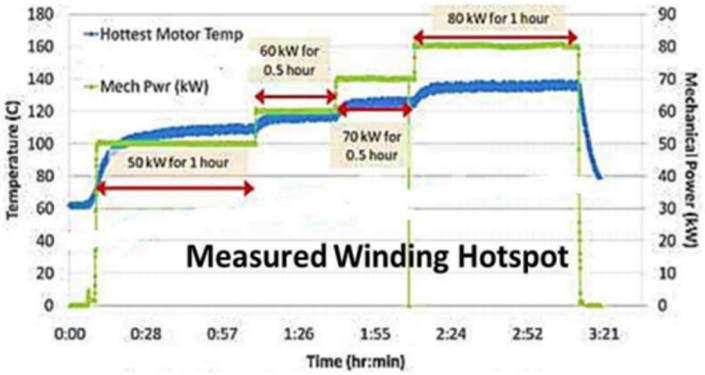

FIGURE 36: 2012 NISSAN LEAF MOTOR'S HOTTEST TEMPERATURE AT POWER AND TIME DEPENDENCE AT 7000 RPM, BASED ON: STATON, GOSS (2017), P. 24

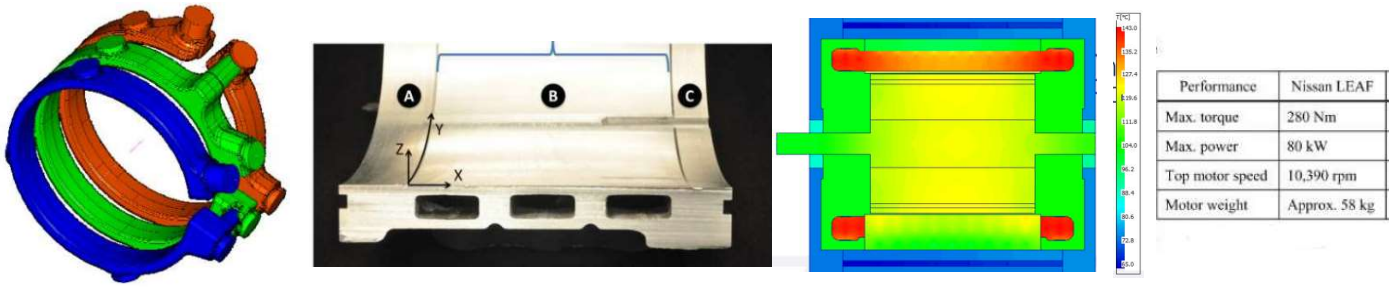

FIGURE 37: WATER JACKET 2012 NISSAN LEAF, BASED ON: STATON, GOSS (2017), P. 11

There are some advanced liquid cooling techniques involving oil as a heat removal fluid. One technique is to drop oil on the rotor so that its rotation throws the liquid around the motor. Electric motor oil cooling offers a chance to merge part of the transmission cooling with the motor cooling. In fact, if the gearbox is located adjacent to the motor housing, a sealed integrated cooling circuit can be designed for both with an auxiliary flow control member to ensure the desired flow of oil on the components.[98]

[97] Conf. Staton; Goss (2017), p. 11.
[98] Conf. Popescu et al. (2016), p. 5.

3.5 Cabin thermal management system

The goal of the thermal management system is to guarantee the comfort of the passengers. The thermal comfort depends on two main groups of factors: measurable factors and personal factors. The first group includes factors like the air flow, the humidity, the temperature and its gradient. The second group comprises the factors which differ from car occupant to car occupant, as for example characteristics of clothes, activity level, age and so on. Taking into account all the factors of these two main groups, it is possible to optimise the goal parameters of the cabin thermal management system.[99]

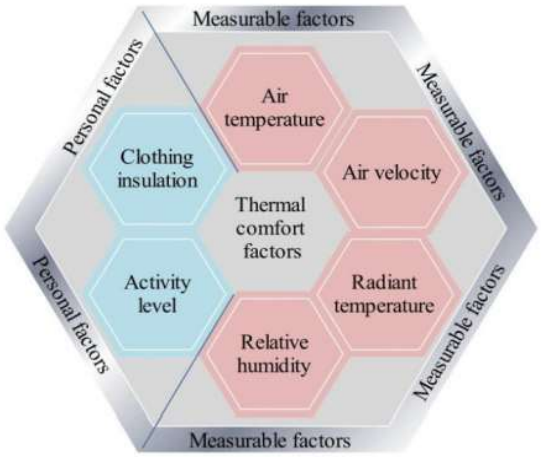

FIGURE 38: THERMAL COMFORT FACTORS DIVIDED INTO MEASURABLE AND PERSONAL FACTORS, SOURCE: SIMION ET AL. (2016), P. 474

If the cabin temperature of ICE vehicles is to be increased, the heat can be taken from the engine which offers an almost unlimited source of heat. In EVs, the most frequently adopted solution is to install a high voltage heater on the air side, although this solution takes away energy from the battery and thus reduces the autonomy range of the vehicle. The Germany-based company MAHLE designs solutions to recover heat from the motor and the battery pack to contribute to the heating of the cabin. The company claims a battery range increase by up to 20% in case the environmental temperature is equal to 0°C. [100]

[99] Conf. Simion; Socaciu; Unguresan (2016), p. 472-478.
[100] Conf. MAHLE (2018), online source [accessed on 19 November 2018].

4 Gear reduction in electric vehicles

With electric vehicles, the term “drivetrain” designates the group consisting of the wheels, the transmission system (shafts, the differential, the gear reduction system) and the electric motor. The drivetrain setup depends on which are the driving wheels and the layout of the power transmission.

The gear reduction system is the mechanical device that changes the speed and the torque coming from the motor to a desired value to transmit on the wheels. The output values are calculated from drive condition requirements which will be described in paragraph (4.2.2). The most common configuration of a gear reduction system consists in a set of rotating gears, linked to a wheel work. The speed and the torque coming in input are converted according to the gear ratio, which will be explained in the next chapter. [101]

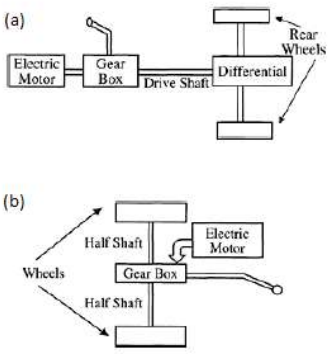

FIGURE 39: TWO DRIVETRAIN CONFIGURATIONS: (A) TYPICAL REAR WHEEL DRIVE, (B) TYPICAL FRONT WHEEL DRIVE, SOURCE HUSAIN (2003), P. 230

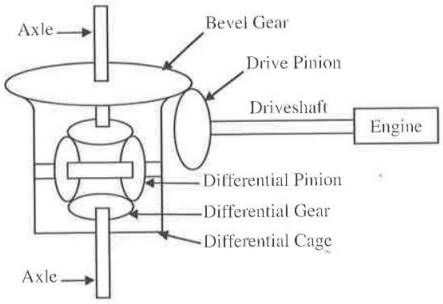

FIGURE 40: SCHEME OF A DIFFERENTIAL, SOURCE HUSAIN (2003), P. 232

[101] Conf. Husain (2003), p. 229.

4.1.1 Physical entities involved in the design of the gear ratio

To introduce the concept of gear ratio, the following definitions are needed. The tangential speed of a body, that is moving in a circular path, is defined as product of the angular velocity of the body and its distance from the centre (the radius). The tangential velocity, as the name suggests, will be always tangential to the radius.

$$v = \omega * r \tag{4.17}$$

Torque (τ), as described in the equation below, is the result of a force (F) applied to a lever (r). Torque is produced when a force is involved in a change of the rotational movement of an object. Torque is expressed in Newton-meters in the SI.

$$\tau = r * F \tag{4.18}$$

Power can be defined as the angular speed multiplied by the torque. In an ideal gearbox (without losses), the input and output power are even. Hence, varying the speed or the torque varies the other one.

$$\omega_{in} * \tau_{in} = \omega_{out} * \tau_{out} \tag{4.19}$$

Theoretically a gearbox can be used to multiply the speed or the torque. However, with electric motors the speed is not multiplied, since it would mean that the motor torque, and consequently the motor size, is unnecessarily oversized.

In the gearbox, there are at least two moving bodies, which mesh with each other and transmit the power through teeth contact, ideally without friction or losses. At the contact point the tangential velocity of the two bodies is the same. Hence, the ratio of radii of the bodies determine the gear ratio.

The gear ratio (GR) can be expressed in the following terms:

$$GR = \frac{\tau_{out}}{\tau_{in}} = \frac{\omega_{in}}{\omega_{out}} = \frac{r_{out}}{r_{in}} \tag{4.20}$$

It is important to know that a gear is fully defined once two parameters are defined: the number of teeth (z) and the module (m) that describes the gear dimension in size unit. From these two parameters it is for example possible to calculate the diameter of the gear:[102]

$$d = m * z \tag{4.21}$$

By referring to the overall gear ratio, the ratio from the motor to the wheel is meant, including, for example, both the gearbox ratio and the differential.

The design of the gear ratio of an electric vehicle is different from a car powered by fossil fuel. Internal combustion engines use the gears to keep the motor in the appropriate power band and to allow the

[102] Conf. Smith; Peterson (1998), p. 249-250.

car to travel at the desired speeds. Depending on whether diesel or gasoline engines are concerned, the torque / rpm curve looks different, but compared to the electric engine curve, the band with a high torque is smaller. In ICEs the gears help to keep the motor running around the optimal point.

Most of the electric mass-produced cars nowadays have a gearbox with a single gear ratio. Electric motors are efficient across a large range of rpm and the torque provided at low rpm is high. The gearbox is needed, in most of the cases, to meet the drive condition requirements, such as top speed, acceleration performance and gradeability torque. The gear ratio has to be designed in order to provide an optimisation of these requirements and of the overall size and costs (of the motor combined with the gearbox).

In case of direct drive, where the motor is not coupled to a gear box but transfers the torque and the speed directly to the wheels or to the differential, the motor has to be sized in order to deliver enough torque to fulfill the above mentioned drive requirements. The optimisation of the overall size and costs means that, thanks to the implementation of a gearbox, it is possible to select a motor with a smaller diameter and a high revving. Hence, the torque will be multiplied and the speed reduced to the desired parameters. This can decrease the costs and optimise the room occupied by the powertrain compared to a direct driven configuration.

4.1.2 Drive condition requirements

The following example shows a possibility of how to design the overall gear ratio with the top speed requirement. The required speed in this case is 200 km/h, with a motor capable to spin at 18000 rpm and a tyre diameter of 0.25 meter. The following equation allows to determine the desired ratio, which is 8.4823 in this case.

$$Overall\ Gear\ Ratio = \frac{RPM}{Top\ Speed} * Tyre\ Circumference \tag{4.22}$$

The mathematical formulation of the acceleration includes a final goal speed (v_f) to be reached within a certain time frame starting from an initial speed (v_i), in a time frame (t_f). The desired acceleration can be obtained as follows:

$$a = \frac{v_f - v_i}{\Delta t} = \frac{v_f}{\Delta t} \tag{4.23}$$

The force that has to provide the acceleration will be called tractive force (F_T) , the force opposing to this movement road is the load resistance force (F_R) and m is the weight of the vehicle. The resistance forces consider: rolling resistance, air resistance, gradient resistance and the inertia. The rolling resistance is related to the wheels rolling on the ground. It describes the resistance of their motion. It is influenced by parameters such as the friction coefficients of the material of the tires and the grounds, the dimensions of the tires, the weight of the vehicle and its speed. The air resistance depends on the geometry of the vehicle and on the wind flow. The inertia is the resistance of the vehicle to the acceleration. This force is given by the mass of the vehicle multiplied by the acceleration required to reach the desired speed starting from the initial one. [103]

The above-mentioned forces can be connected to the vehicle acceleration with this equation:

$$a = \frac{dv}{dt} = \frac{F_T - F_R}{m} \tag{4.24}$$

Once the required tractive force is known, the tractive torque required can be calculated as follows:

$$\tau_T = F_T * r_{wh} \tag{4.25}$$

[103] Conf. Vuchic (2007), p. 92-97.

This torque divided by the number of driving wheels indicates the torque required after the overall gear ratio, and hence, it is possible to obtain a second parametric equation to calculate the gear ratio needed.

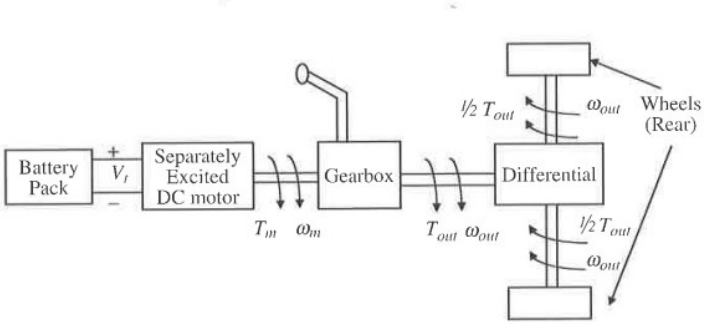

FIGURE 41: TORQUE AND SPEED THROUGH A DRIVETRAIN OF AN EV, SOURCE HUSAIN (2003), P. 232

A further requirement for the gear ratio selection is about the maximum gradeability. It is the highest slope inclination that a vehicle can ascend. Assuming that the car is moving without accelerating, the resistances to the vehicle movement are the same as for the previous case, which are: rolling resistance, air resistance, gradient resistance. By adopting the angle of inclination of the slope as a variable it is possible to determine the required torque as before, and thus the gear ratio. [104]

[104] Conf. Yamsani (2014), p. 35.

4.2 Layout of the gear ratio reduction system

By designing and choosing which type of gearbox to use, different factors have to be taken into account, among them the layout of the powertrain, the motor technology, the type of drive, the room available.

Talking about the layout of the motor, it has to be considered how the motor is set into the body-frame of the vehicle: either in a transverse or in a longitudinal position. These directions relate to the direction of the movement of the vehicle. Transverse motor setups are a common choice for utilitarian cars. Having a transverse engine means that its axis is parallel or co-axial to the wheels' shaft. The longitudinal configuration is not so common in utilitarian cars due to the dimensions of the front and back hoods. The longitudinal design is a good solution for the Formula-E cars because of the shape of the car-body. This solution requires a reduction gear which transfers the power at 90°.

FIGURE 42: TRANSVERSE MOTORS IN TESLA´S DUAL MOTOR ALL WHEEL DRIVE, ONLINE SOURCE: TESLA (2018), [ACCESSED ON 20 NOVEMBER 2018]

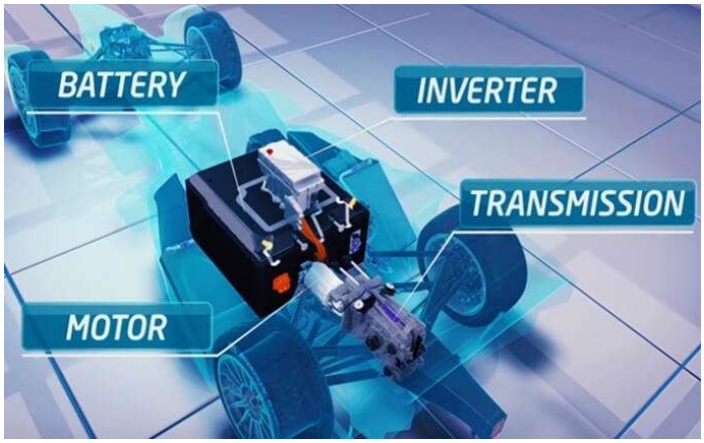

FIGURE 43: LONGITUDINAL ENGINE ON A FORMULA E CAR, ONLINE SOURCE: ABB FORMULA E (2016), [ACCESSED ON 20 NOVEMBER 2018]

During the design of a transmission, the type of drive needs to be considered. According to Naunheimer et al. (2011) front-wheel drive is the most frequently chosen mode for ICE vehicles, though sports cars often adopt the rear-motor drive. All-wheel drives have been getting more popular in the last years and this configuration can be found in almost any current vehicle series. The same trend can be forecast with certainty for electric vehicles.[105]

Configuration		Drive		
		Front	Rear	Front + Rear
Engine	Front	Front-wheel drive	Standard drive	4-wheel drive
	Rear	Not practicable	Rear-motor drive	4-wheel drive

TABLE 4: POSSIBLE DRIVE CONFIGURATIONS, SOURCE NAUNHEIMER ET AL. (2011), P. 141

Several components of the drivetrain are influenced by the drive architecture. Table 5 shows some of them and their interaction.

Parameters	Configurations (passenger car)				
Position of engine	Front – longitudinal	Front – transverse	Rear – longitudinal	Rear – transverse	_____
Driven axle(s)	Front-wheel drive	Rear-wheel drive	4-wheel drive	_____	_____
Position of engine relative to gearbox	Engine in front of gearbox	Engine behind gearbox	Engine above gearbox	Engine beside gearbox	Engine longitudinal, gearbox transverse (T configuration)
Position of engine and gearbox relative to final drive	Engine, gearbox and final drive as a block	Final drive separate from engine and transmission (standard drive)	Engine separate from gearbox and final drive	_____	_____
Gearbox/final drive structurally combined	Final drive integral to gearbox	Final drive flange-mounted to gearbox	Gearbox and final drive separate	_____	_____
Final drive	Spur gears	Bevel gear helical bevel drive	Bevel gear hypoid bevel drive	Worm gears	Belt drive
Differential lock	Unlocked	Self-locking	Manual locking	Electronic locking	_____
Differential gear	Spur gears	Bevel gears	Helical gears	Worm gears	_____

TABLE 5: MORPHOLOGICAL MATRIX FOR PASSENGER CAR POWERTRAINS, BASED ON NAUNHEIMER ET AL. (2011), P.141

[105] Conf. Naunheimer et al. (2011), p. 141.

4.3 Transmission technologies

In order to achieve the desired gear ratio, an appropriate gearbox technology has to be chosen. Beside direct drives, possible solutions are spur gears, planetary gearboxes, belt pulley transmissions.

4.3.1 Direct-drive

A direct-drive can be adopted in heavy duty vehicles with high torque and low speed motor. Heavy duty vehicles usually do not have challenging specifications regarding the volume occupied by the powertrain. According to Olivier Bernatchez, Channel and Account Manager at TM4 Inc., direct-drive configuration can be the best compromise between efficiency and simplicity. Gearless solutions have the advantage of a higher efficiency due to the absence of the gearbox. TM4 adopted the direct-drive solution for some motors for commercial vehicles (such as medium and heavy-duty trucks and buses). It was found out that a design including a gearbox would have been more expensive and would have increased the complexity of the system, because of the high torque required on the wheels. Additional advantages according to Bernatchez, are a higher simplicity of installation and an easier incorporation of a new electric powertrain in already existing vehicle designs. Less components mean a direct increase in reliability and a reduction of maintenance. According to Bernatchez "Our direct-drive motors, if used in the conditions prescribed by TM4, will last 1 million kilometres without any maintenance being required". To sum up, direct drive can be the best solution in applications where the goal is the best torque density considering the costs in the long and short term. [106]

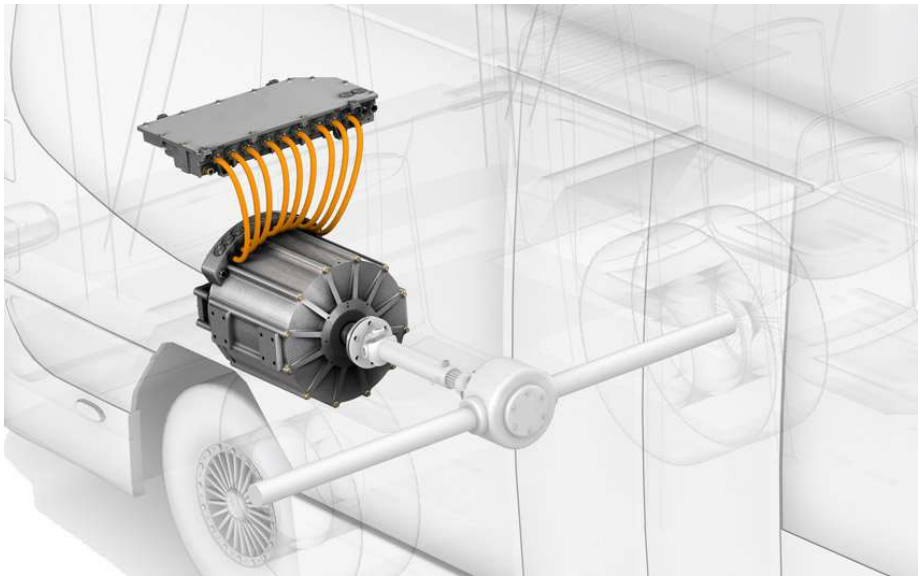

FIGURE 44: DIRECT-DRIVE CONFIGURATION ON A HEAVY DUTY VEHICLE, ONLINE SOURCE: TM4 (2018), [ACCESSED ON 20 NOVEMBER 2018]

[106] Conf. Bernatchez (2016), online source [accessed on 20 November 2018].

4.3.2 Gears

Gears are one of the most adopted solutions to achieve the required ratio. Advantages of this solution are reliability and small dimensions. Gears can transmit the torque over different angles, typical configurations are on 90° shafts and on parallel shafts. Disadvantages are weight and need of lubrication. As described in chapter 2, electric vehicles often use regenerative braking systems to recharge the battery. It is possible to induce electricity in the stator letting the rotor rolling in the opposite direction compared to when energy is transferred from the battery to the wheels. In this way, the EM acts like a generator and recharges the battery. To achieve this, the reduction system has to be able to transmit the torque coming from the wheels to the motor shaft. Gears are suitable for this application.[107]

In the following paragraphs the most frequently adopted gearing solutions are described by quoting SDP/SI, a manufacturing company of precision gears and gear assemblies.[108]

There are different layouts available for transmitting the torque on a 90° angle: screw gears, straight bevel gears, spiral bevel gears, zerol gears, hypoid gears, worm sets and double enveloping worm gears.

Screw gears can be designed by using crossed helical gears. Helical gears can be used to transmit power to parallel axis. Although setting two of those, which have opposite helix angles, on a cross axis can work as a 90° transmission and it is defined as a screw gear layout. The load carrying capacity of screw gears is rather restricted.

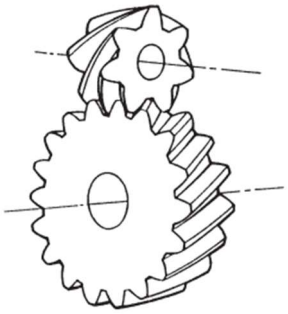

FIGURE 45: SCREW GEARS USING CROSSED HELICAL GEARS, SOURCE: SDP/SI (2018), P. 1

[107] Conf. Tort (2016), p. 6.
[108] Conf. SDP/SI (2018), p. 1.

Straight bevel gears have a conical pitch surface and have a straight tooth geometry. The teeth have the same direction as the pitch cone base line (generatrix). Straight bevel gears are both the most commonly applied from the bevel gear family and the easiest to produce.

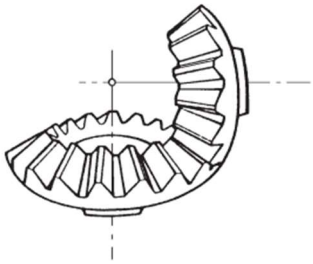

FIGURE 46: STRAIGHT BEVEL GEARS, SOURCE: SDP/SI (2018), P. 1

Spiral bevel gears have a helical angle of spiral teeth. The manufacturing process is more complex, however these gears offer higher strength and lower noise compared to the straight bevel design.

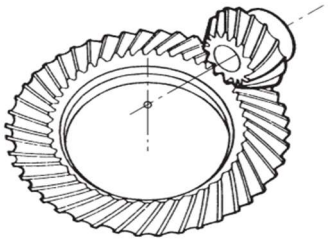

FIGURE 47: SPIRAL BEVEL GEARS, SOURCE: SDP/SI (2018), P. 1

A zerol gear is a specific case of spiral bevel gear, in fact it is a spiral bevel gear with the angle of the spiral equal to 0°. Its axial thrust is lower compared to the one of spiral bevel gears.[109]

FIGURE 48: ZEROL GEAR, TKK CORPORATION (2018), ONLINE SOURCE [ACCESSED ON 19 NOVEMBER 2018]

[109] Conf. TKK Corporation (2018), online source [accessed on 19 November 2018].

The hypoid gear was developed for the automobile industry. It is similar to the spiral bevel gear, except that the axes of the two elements do not intersect, which leads to the possibility of lowering the body frame of the car. The manufacturing of these gears is complex and requires more expensive machines compared to the previously seen gears.

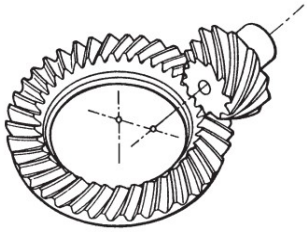

FIGURE 49: HYPOID GEAR, SOURCE: SDP/SI (2018), P. 1

A worm set is a gear which is composed of a worm and a worm gear. The term worm is used to designate a screw thread while the worm gear is the meshing helical gear. The special characteristic of this gearing is the high ratio available, although the drawback is a poor efficiency due to high friction between the worm and the gear. Special attention to the lubrication and to the materials is required in order to reduce wear.

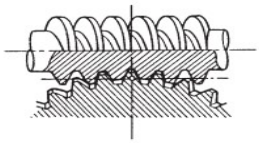

FIGURE 50: WORM SET, SOURCE: SDP/SI (2018), P. 1.

Double enveloping worm gears are an advanced version of the single enveloping ones. Their advantages are higher load capacity and tighter architectures. Disadvantages are a more demanding machining with higher costs and a more complex assembly of the set.

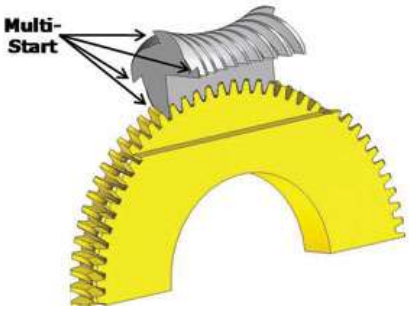

FIGURE 51: DOUBLE ENVELOPING WORM GEAR, ONLINE SOURCE: PIERROTTI (2012), [ACCESSED ON 20 NOVEMBER 2018]

The most common gears used for transmitting the torque on parallel axes are: spur gears, helical gears and double helical gears.

A spur gear has a cylindrical shape with the teeth parallel to the axis. It has a wide range of applications and its manufacturing process is relatively simple.

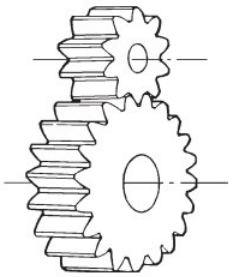

FIGURE 52: SPUR GEARS, SOURCE: SDP/SI (2018), P. 1

Helical gears have a cylindrical shape with helicoidal teeth. Thanks to the teeth shape they can stand higher loads compared to the spur gears and they generate less noise during working. Drawbacks are higher costs and the generation of an axial thrust force due to the helix form.

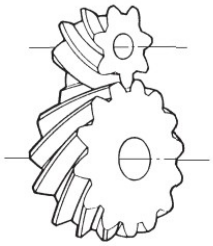

FIGURE 53: HELICAL GEARS, SOURCE: SDP/SI (2018), P. 1

An evolution of the previous gear is represented by the double helical gear. It has both left-hand and right-hand helical teeth. This layout balances the inherent thrust forces.

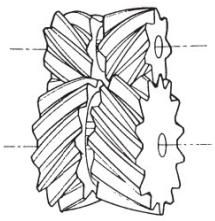

FIGURE 54: DOUBLE HELICAL GEARS, SOURCE: SDP/SI (2018), P. 1

4.3.3 Belt and pulley systems

This type of transmission is made with two pulleys and one belt running on them. The driver pulley is connected to the axle of the motor and the driven pulley is connected to the wheel shaft. Advantages of this system are less weight and the fact that no lubrication is required. Disadvantages are that it occupies more room, that it has a lower reliability compared to the geared solution and that usually it has a lower efficiency. The belt system is rarely adopted, since the room in the powertrain is a critical factor. Applications where the distance between the power and the driven shaft are fix and considerably elevated are suitable for this type of transmission.[110]

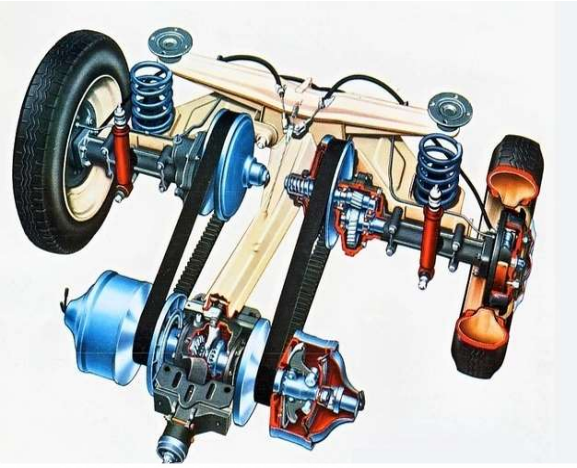

FIGURE 55: DAF´S CONTINUOUSLY VARIABLE TRANSMISSION, ONLINE SOURCE: AUTORAI (2018), [ACCESSED ON 20 NOVEMBER 2018]

A transmission technology that uses belts and pulleys is the CVT transmission. CVT is an acronym that stands for Continuous Variable Transmission. The ratio is continuously adjusted over the range allowed by its design. It can be defined a primary side, on which the belt receives the input from the motor through a clutch. The belt is then connected to the final drive through gears, that is called the secondary side.[111]

The principle of the changing ratio of the CVT system is the following: When the required ratio is higher, the circumference on the primary side increases while the circumference on the secondary side decreases. Vice versa, when a lower transmission ratio is required, the circumference of the driven pulley increases and the circumference of the drive pulley increases. The movement of the pulleys is usually controlled by hydraulic pumps and reacts fast to the changes given in input by the driver. The pulleys are adjusted in order to remain within the most efficient rpm range. This solution was adopted for example for 2013 Nissan Altima and 2012 Scion iQ.[112]

[110] Conf. Tort (2016), p. 6.
[111] Conf. Miller (2010), p. 96.
[112] Conf. Winnipeg Synthetics (2018), [accessed on 20 November 2018].

4.3.4 E-CVT

The E-CVT (electronically-controlled continuously variable transmission) does not use neither pulleys nor belts. To perform the gear reduction at least one set of planetary gearing is used.

4.3.4.1 Planetary gearing

A planetary gearing consists of the parts shown in figure 58: the sun, the planets, the carrier and a ring. A movable arm, the carrier, supports the planets during their rotation around the sun. The planetary gear teeth are meshing with the ones of the sun gear and of the ring gear, engaging the teeth with both. Hence the angular velocity of the carrier, depends on the movement of the sun and of the ring. The sun is usually connected to the motor shaft and the speed of the ring is controlled electronically. Compared to parallel axis gearing, planetary gears offer high reduction ratio in smaller volume, higher power density and coaxial shafting which can be an advantage depending on the powertrain configuration. On the other hand, parallel axis gearings are usually characterized by a less complex design and a better accessibility. Planetary gearings are characterized by high efficiency; in fact, with typical gearing stages losses of around 3% occur. Moreover, this type of gearing has a high torque capacity thanks to the planet configuration which transfers the load from the sun to the planets. Increasing the number of planets leads to a higher torque density and improves the load capacity. [113]

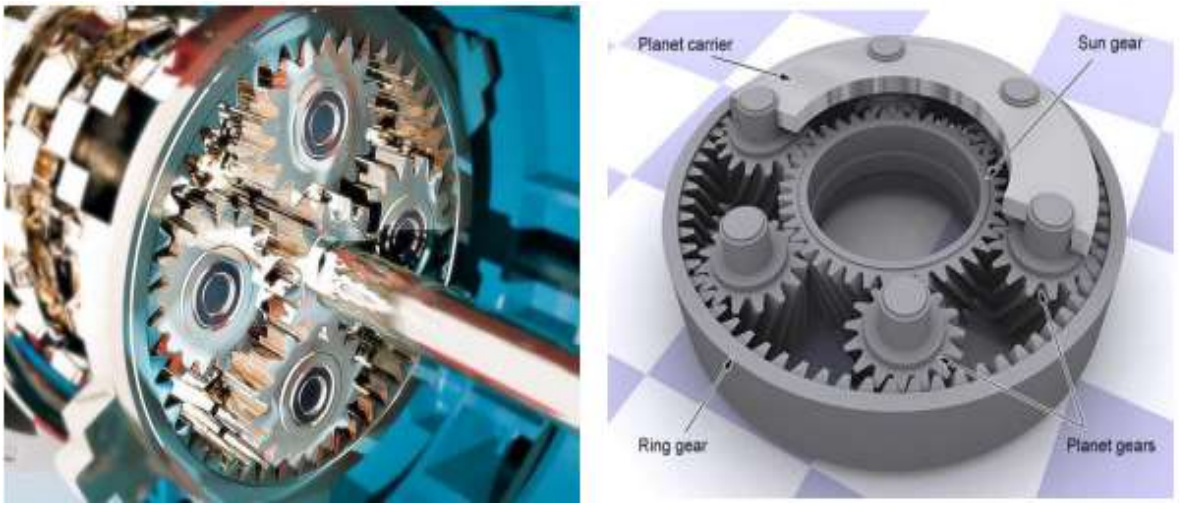

FIGURE 56: PLANETARY GEARING, SOURCE: CORBELLI (2011), P. 13

[113] Conf. Corbelli (2011), p. 13-14.

The following paragraphs explain some of the most relevant physical entities and the relationships between the speeds of the mechanical parts of the planetary gearing.

The relationship between the radius of the sun (r_s), the radius of the planets (r_P) and the internal radius of the ring (r_R) can be described as in equation (4.26). Figure 57 represents this relationship graphically.

$$r_R = r_s + 2 * r_P \tag{4.26}$$

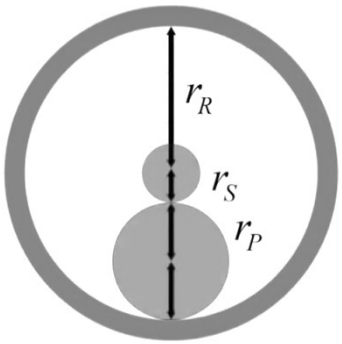

FIGURE 57: RADII IN PLANETARY GEARING, SOURCE: OWN ILLUSTRATION

It is possible to rewrite this equation as follows:

$$2 * r_P = r_R - r_s \tag{4.27}$$

Assuming for example that the sun is adopted as input and the carrier as output, the gear ratio (i) can be written in this case as the ratio of the angular velocity of the sun (ω_s) on the angular velocity of the carrier (ω_c):

$$GR = \frac{\omega_s}{\omega_c} \tag{4.28}$$

Corresponding to the steps of the attachment (9.4) which use the definition of linear velocity for a body moving in a circle path, it is possible to rewrite the gear ratio as follows:

$$GR = 1 + \frac{R_R}{R_s} \tag{4.29}$$

Since the radii are proportional to the number of teeth, it can be derived:

$$GR = 1 + \frac{Z_R}{Z_s} \tag{4.30}$$

The parameter (Γ) describing the planetary gearing teeth, defines the ratio between the number of teeth of the ring (R) and the number of teeth of the sun (S) as follows:

$$\Gamma = -\frac{Z_R}{Z_S} \tag{4.31}$$

This transmission ratio depends on the speed of the sun (ω_S) and the ring (ω_R) in relation with the speed of the carrier (ω_C). Hereinafter is the derivation of the previous equation:

$$\tau = \frac{\omega_{SC}}{\omega_{RC}} = \frac{\omega_S - \omega_C}{\omega_R - \omega_C} = -\frac{Z_R}{Z_S} \tag{4.32}$$

Since the center axes of the ring and of the sun have to be coincident and since planet gears have the same module in most application cases, it is possible to derive an equation connecting the number of teeth of the ring (R), with the number of teeth of the sun (S) and the number of teeth of the planets (P):

$$Z_R = Z_S + 2 * Z_P \tag{4.33}$$

4.3.4.2 E-CVT in hybrid vehicles

One means to combine/split the power sources in parallel hybrids is the electronic continuously variable transmission (E-CVT). The E-CVT allows working at the optimal working point by keeping a varying reduction ratio and this leads to better fuel economy and to a reduction of inefficiencies. In contrast to the belt-pulley CVT technology, E-CVT offers the possibility to apply power coming from different sources on one output axis. At least one planetary gearing is used to merge the power coming from the ICE and electric motor/generator by means of clutches. In one of the possible configurations the ICE is connected to the planet gear by a clutch, while another clutch attaches the sun to the motor/generator with the ring gear being the output of the system. This architecture is shown in figure 60. [114]

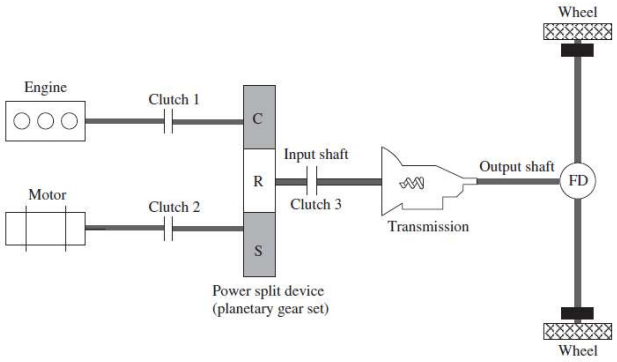

FIGURE 58: EXAMPLE OF E-CVT IN HYBRID POWERTRAIN, SOURCE LIU (2017), P. 78

An energy management algorithm is implemented to switch on and off the different clutches and to allow the power flowing through the planetary gearing. Each part of the gearing can be kept static, can be allowed to rotate freely, or a power source can be activated. Considering the specific case where the full hybrid mode is switched on by the energy management, the clutches engage both the electric motor/generator and the internal combustion engine. In case no losses occur, the following equations can be defined according to Liu (2017). [115]

[114] Conf. Liu (2017), p. 78.
[115] Conf. Liu (2017), p. 67.

The following equation shows the relation between the speeds of the gears in the planetary gearing of the E-CVT in case all clutches are engaged:

$$\omega_S + \omega_R * \frac{Z_R}{Z_S} - \left(1 + \frac{Z_R}{Z_S}\right) * \omega_C = 0 \tag{4.34}$$

The power in output from the E-CVT ($P_{E-CVT,out}$) is equal to the power produced by the electric motor (P_{EM}) and the power produced by the internal combustion engine (P_{IC}):

$$P_{E-CVT,out} = P_{IC} + P_{EM} \tag{4.35}$$

The rotation speed of the E-CVT output axle is the same as the one in input on the transmission (see Figure 58). The following equation can be derived from the radii of the planetary gearing and the output velocities of the ICE and of the EM:

$$\omega_{E-CVT,out} = \left(\frac{r_R + r_S}{r_R}\right) * \omega_{ICE} - \frac{r_S}{r_R} * \omega_{EM} \tag{4.36}$$

The torque in output from the E-CVT is the same which acts on the input of the transmission (see figure 60Figure 58). It can be derived from the power of the ICE and of the EM and their velocities as in the following equation:

$$\tau_{E-CVT,out} = \frac{P_{EM}}{\omega_{mot}} - \frac{P_{ICE}}{\omega_{ICE}} \tag{4.37}$$

Toyota Motor Corporation has registered a powertrain technology under the name Hybrid Synergy Drive System which implements the E-CVT in hybrid configuration. In figure 61, three gear systems of Toyota are shown. All three are based on the powertrain explained above. The three are implemented in different Toyota vehicles and represent an evolution driven by optimisation. Quoting Katsuaki Watanabe, the CEO of Toyota, this third generation aims at halving size and costs of the HSD system [116].

In all three configurations a generator is connected through a hollow rotor shaft to the sun gear of the planetary gear where the ICE is linked to the carrier. In the version of the first generation a chain system is used to connect the output shaft of the planetary ring to the counter drive gear, while in the second generation version foresees the planetary ring meshing directly with the counter drive gear.[117]

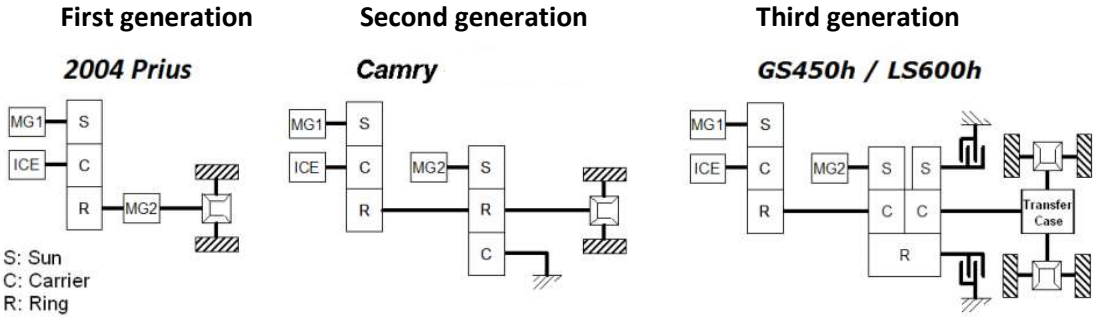

FIGURE 59: DIAGRAM OF THREE E-CVT SYSTEMS OF TOYOTA, BASED ON BURRESS ET AL. (2011), P. 38

[116] Conf. BusinessWeek (2007), online source [accessed on 26 November 2011].
[117] Conf. Burress et al. (2011), p. 37-41.

4.4 Number of gear stages

Once the gear ratio and the gear technology are chosen, the gear stages can be defined and optimized. The number of stages is usually counted taking the number of axis minus one. Using a number of gear stages greater than one, has the advantage that the desired gear ratio can be achieved by combining the individual ratios. For example, to achieve a gear ratio of 25:1 with a two-stage gear, two steps of 5:1 can be implemented.

The aims of this phase are to design the transmission as light as possible by optimizing the room occupied and to achieve the highest possible efficiency.

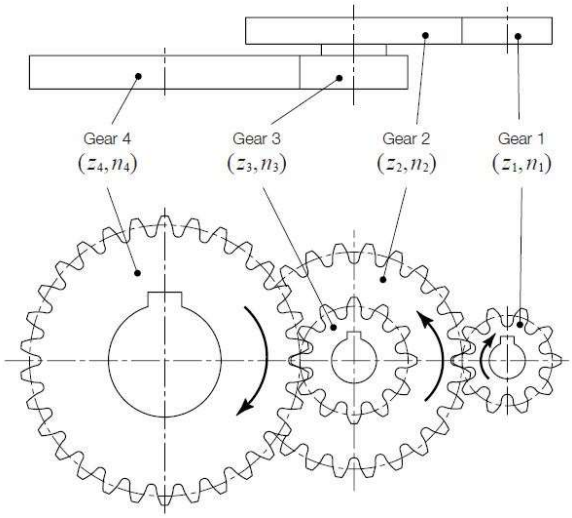

FIGURE 60: EXAMPLE OF A TWO-STAGE GEAR SYSTEM, ONLINE SOURCE KH GEARS (2018), [ACCESSED ON 26 NOVEMBER 2018]

4.5 Future of transmission in EVs

Electric motors are highly efficient and the coupling with one speed transmission usually is enough to achieve the torque required to move a vehicle from the standstill point throughout the whole speed range till the maximum speed is reached.

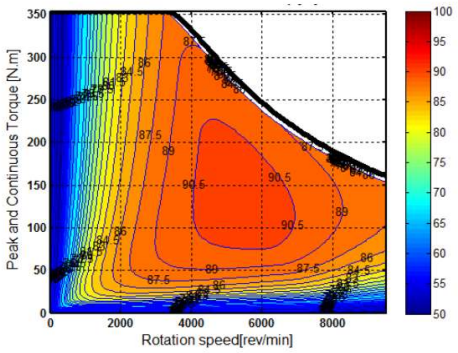

FIGURE 61: EFFICIENCY MAP OF AN EM FOR THE AUTOMOTIVE INDUSTRY, SOURCE BADIN ET AL. (2015), P. 4

In literature, the possibility of multi-speed transmissions for electric motors is widely analysed. The advantages of such an architecture can be a reduction of energy consumption and an increase of the dynamic performances. The highest level of efficiency of an electric motor is usually obtained in the area of medium load and medium/high speed, a multi-speed transmission can help the motor keep working at optimal efficiency, as shown in figure 64.

The dynamic performances which can be improved by adopting a multi-speed transmission, are the maximum speed and the initial torque. For example, a two-speed transmission compared to a one-speed transmission, can have a first gear with a higher ratio in order to increase the initial torque and a second one smaller in order to increase the maximum speed.

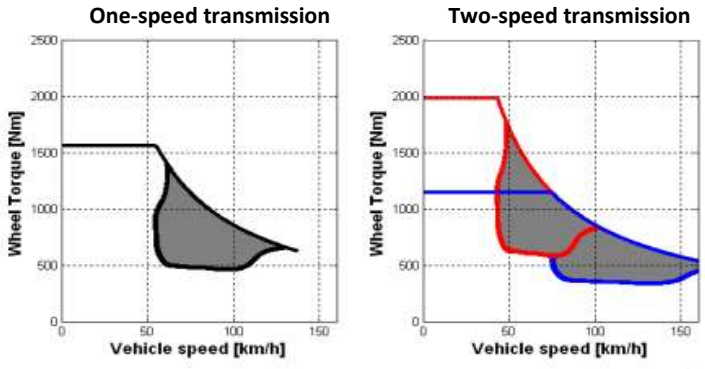

FIGURE 62: SPEED-TORQUE MAP OF A MOTOR WITH ONE-SPEED TRANSMISSION (ON THE LEFT) AND WITH TWO-SPEED TRANSMISSION (ON THE RIGHT), BASED ON FAID (2015), P. 6

Multi-speed transmission solutions are adopted in Formula E cars in order to achieve the highest possible performance following the rules imposed by the International Automobile Federation for the specific season. Another example for a vehicle adopting multi-speed transmission is the supercar Concept One designed and manufactured by the company Rimac. The choice not to adopt multispeed transmissions in ordinary full EVs is due to the increase of weight, to major complexity and higher costs that a multi-speed transmission solution requires.

5 Conclusions

The current layouts of BEVS and HEVs are explained and a projection of their market share is outlined according to different scenarios based on the policies of the countries. Different areas of an electric vehicle are looked at including powertrain, battery pack and thermal management. The technologies adopted are described and advantages and disadvantages are considered. According to the forecasts, the electrification in the automotive industry will grow rapidly in the next two decades and the market share of BEVs and HEVs in ten years from the moment of this writing will be almost even. The production of EVs is expected to be a mass production and hence high specialised machineries can be adopted. It can be expected that in HEVs the contribution to the propulsion of the EM will increase in the years. A design of interchangeable parts between HEVs and BEVs will allow benefits of economy of scale.

A new generation of batteries is likely to be on the market in the time step considered. The most promising is the Li-S battery, which might lead to energy densities in the range of 500-600 $Wh*Kg^{-1}$, compared to the value of approximately 220 $Wh*Kg^{-1}$ of the current Li-ion batteries. Before the market entry of a new technology, it is supposed to see a growth in energy density of the Li-ion batteries combined with bigger battery packs in order to increase the autonomy range. The increase of the energy of the battery pack requires a higher heat removal ratio. The thermal management system has to be designed to keep the battery in its optimal thermal range, which depends on the battery technology. The temperatures of Li-ion batteries must not exceed values of approximately 60°C in order to avoid the risk of initiating reactions, which could lead to permanent damages in the pack and ignite a combustion process. Irreversible capacity fading was observed at cycling Li-ion batteries at low temperatures (5°C). This phenomenon was due to the formation of layers impeding the diffusion of Li-ions diffusion. Hence, during the charging and discharging process heat has to be provided to the battery pack. The design of the thermal management system of the cells is driven by the geometry cells adopted. Due to the low performances, air cooling systems will most likely be abandoned in favour of liquid cooling systems with the interaction of fins for pouch and prismatic cells, whereas ribbons are used for cylindrical cells. Dielectric cooling fluid can be expected to be commonly adopted in race and in sports cars. Dielectric fluid can be used in direct cooling, which improves the uniformity of the temperature over the cell and requires a simpler system of pipes, which entails another advantage, namely lower weight. On the other hand, dielectric fluids are more expensive and the cases in which the fluid flows have to be leakage free.

The motor technology adopted by the largest number of car producers is PMM. The reason for this development is its efficiency compared to induction motors. In PPMs the maximum working temperature is ensured by the magnet; in fact, at the Curie temperature irreversible demagnetisation occurs. In order to allow the motor to work with high loads for long periods it has to be cooled. The methods with the highest removing heat ratio involve direct oil cooling on the rotor. Simpler but less effective solutions are cooling systems on the housing of the motor.

It was seen that the integration of the thermal management systems (battery, cabin, electronic and motor) can increase the autonomy range up to 20% in case the environmental temperature is equal to 0°.

The characteristic curve of electric motors differs radically from the curve of internal combustion engines. The electric motor is considerably more efficient and produces high torque over the entire rpm range. A gearing can be used to multiply the torque and to reduce the output speed. The design of the gearing is determined by the pursuit of cost optimisation and by the motor dimension and by the transmission type. In vehicles where the dynamic performances have the priority over costs, a multi-step gear ratio ensures better acceleration, top speed and efficiency, even if, on the other hand, a heavier and more complex system is required.

6 Bibliography

Ajanovic, Amela (2015): “The future of electric vehicles: Prospects and impediments.” In: Wiley Interdisciplinary Reviews: Energy and Environment, 4 (2015), H. 6, p. 521–536. Available at: DOI: 10.1002/wene.160

Anderson, Curtis D.; Anderson, Judy (2010): Electric and Hybrid Cars: A History.

Arnott, Neil (1877): Elements of Physics Or Natural History. Appleton.

AVID Technology (2018): PM Radial Flux Motors. Available at: URL: https://avidtp.com/product/pm-radial-flux-motors/[Accessed on: 15 November 2018].

Badin, F; Le Berr, F; Castel, G.; Dabadie, JC; Briki, H.; Degeilh, P; Pasquier, M. (2015): Energy efficiency evaluation of a Plug-in Hybrid Vehicle under European procedure, Worldwide harmonized procedure and actual use. EVS28 International Electric Vehicle Symposium and Exhibition.

Badran, Omar; Sarhan, Hussain; Alomour, Bilal (2012): “Thermal performance analysis of induction motor.” In: International Journal of Heat and Technology, 30 (2012), H. 1, p. 75–88. Available at: URL: https://www.researchgate.net/publication/289032931

Bandhauer, Todd M.; Garimella, Srinivas; Fuller, Thomas F. (2011): “A Critical Review of Thermal Issues in Lithium-Ion Batteries.” In: Journal of The Electrochemical Society, 158 (2011).

Barnes, Malcolm (2003): Practical Variable Speed Drives and Power Electronics. Newnes.

Bernardi, D.; Pawlikowski, E.; Newman, J. (1985): “A General Energy Balance for Battery Systems.” In: Journal of The Electrochemical Society, 132 (1985).

Bernatchez, Olivier (2016): 5 advantages of a direct-drive motor. Available at: URL: https://www.tm4.com/blog/benefits-removing-transmission-commercial-vehicle/[Accessed on: 20 November 2018].

Blain, Loz (2017): One-megawatt electric on/off-road Miss R supercar. Available at: URL: https://newatlas.com/xing-miss-r-on-off-road-electric-hypercar/52317/[Accessed on: 25 November 2018].

Boldea, Ion; Nasar, Syed A. (2002): The Induction Machine Handbook. CRC Press.

Bonnett, Austin H. (2001): “Operating Temperature Considerations and Performance Characteristics for IEEE 841 Motors.” In: IEEE TRANSACTIONS ON INDUSTRY APPLICATIONS, 37 (2001).

Bower, George (2018): Tesla Model 3 Battery Cooling Much-Improved. Available at: URL: https://insideevs.com/tesla-model-3-battery-cooling-track-mode/[Accessed on: 25 November 2018].

Burress, T. A. et al. (2011): EVALUATION OF THE 2010 TOYOTA PRIUS HYBRID SYNERGY DRIVE SYSTEM. UT–Battelle.

BusineesWeek (2007): Toyota’s Bid for a Better Battery. Available at: URL: https://web.archive.org/web/20070228120107/http://www.businessweek.com/magazine/content/07_10/b4024075.htm

Chen, Dafen et al. (2016): “Comparison of different cooling methods for lithium ion battery cells.” In: Applied Thermal Engineering, 94 (2016).

Cheng, Kwo Chang et al. (1999): Advances in Cold-Region Thermal Engineering and Sciences. Springer-Verlag Berlin Heidelberg.

Cheng, Shukang et al. (2012): Research on Induction Motor for Mini Electric Vehicles. Energy Procedia , p. 249–257. Available at: DOI: 10.1016/j.egypro.2012.02.091

Corbelli, Piero (2011): Hybrid e-CVT Power Split Drivelines.

Corbo, Pasquale; Migliardini, Fortunato; Veneri, Ottorino (2011): Hydrogen Fuel Cells for Road Vehicles. Springer.

Cox, Jim (2007): Electric Motors. Trans-Atlantic Publications.

Day, Lance; McNeil, Ian (1998): Biographical Dictionary of the History of Technology. Routledge.

Eckl, Richard et al. (2013): Conference on Future Automotive Technology: Focus Electro Mobility. Edited by Markus Lienkamp. Springer.

Erriquez, Mauro et al. (2017): Trends in electric-vehicle design. McKinsey & Company. Available at: URL: https://www.mckinsey.com/industries/automotive-and-assembly/our-insights/trends-in-electric-vehicle-design

EV Volumes (2018): No Title. Available at: URL: http://www.ev-volumes.com/country/total-world-plug-in-vehicle-volumes/[Accessed on: 11 November 2018].

Faid, Saphir(2015): Highly Efficient Two Speed Transmission for Electric Vehicles.

Fayyad, Sayel M. et al. (2012): “Optimization of the Electrical Motor Generator in Hybrid Automobiles.” In: Adv. Theor. Appl. Mech., 5 (2012), H. 3, p. 145–159.

Finley, William R.; Hodowanec, Mark M. (2001): “Selection of copper versus aluminum rotors for induction motors.” In: IEEE Transactions on Industry Applications, 37 (2001), H. 6, p. 1563–1573. Available at: DOI: 10.1109/28.968162

French, Daniel (2017): When They Hid the Fire: A History of Electricity and Invisible Energy in America. University of Pittsburgh Press.

Gieras, Jacek F.; Wing, Mitchell (2002): Permanent magnet motor technology: design and applications. Marcel Dekker.

Hall, Carl W. (1999): Laws and Models: Science, Engineering, and Technology. CRC Press.

Hawley, George (2017): Understanding Tesla’s lithium ion batteries. Available at: URL: https://evannex.com/blogs/news/understanding-teslas-lithium-ion-batteries[Accessed on: 25 November 2018].

Hewson, John C.; Domino, Stefan P. (2015): Thermal runaway of lithium-ion batteries and hazards of abnormal thermal environments.

Holzer, Holger (2018): “Die Rückkehr des Wechselakkus.” In: Zeit Online, (2018). Available at: URL: https://www.zeit.de/mobilitaet/2018-12/elektromobilitaet-wechsel-akkus-elektroauto-rueckkehr-zukunft[Accessed on: 23 December 2018].

Huisman, Jaco; Söderman, Maria Ljunggren; Tertre, Francois (2017): Prospecting Secondary raw materials in the Urban mine and Mining wastes.

Hunt, Ian A. et al. (2016): “Surface Cooling Causes Accelerated Degradation Compared to Tab Cooling

for Lithium-Ion Pouch Cells.” In: Journal of The Electrochemical Society, 163 (2016).

Husain, Iqbal (2003): Electric and Hybrid Vehicles: Design Fundamentals. CRC Press.

International Energy Agency (2018): " Global EV Outlook 2018". Available at: URL: https://www.iea.org/gevo2018/[Accessed on: 11 November 2018].

Ismail, Nur Hazima Faezaa et al. (2014): “Simplified Heat Generation Model for Lithium ion battery used in Electric Vehicle.” In: Materials Science and Engineering, 53 (2014).

Jandaud, Pierre-Olivier; Le Besnerais, Jean (2017): Heat transfer in electric machines.

Kam, Kinson C.; Doeff, Marca M. (2012): Electrode Materials for Lithium Ion Batteries. Available at: URL: https://www.sigmaaldrich.com/technical-documents/articles/material-matters/electrode-materials-for-lithium-ion-batteries.html[Accessed on: 23 November 2018].

Kaviany, Massoud (2011): Essentials of Heat Transfer: Principles, Materials, and Applications. Cambridge University Press.

Khajepour, Amir; Fallah, M. Saber; Goodarzi, Avesta (2014): Electric and Hybrid Vehicles: Technologies, Modeling and Control - A Mechatronic Approach. Wiley.

KIT (2018a): The invention of the electric motor 1800-1854. Available at: URL: http://www.eti.kit.edu/english/1376.php[Accessed on: 8 November 2018].

KIT (2018b): The invention of the electric motor 1856-1893. Available at: URL: https://www.eti.kit.edu/english/1390.php[Accessed on: 21 November 2018].

Liu, Wei (2017): Hybrid Electric Vehicle System Modelling and Control.

Lu, Z. et al. (2015): “Thermal Management of Densely-packed EV Battery Set.” In: EVS28 International Electric Vehicle Symposium and Exhibition.

Mackay, Jennifer (2011): Electric Cars. Gale Cengage Learning.

MAHLE (2018): MAHLE thermal management: enabler for electromobility. Available at: URL: https://www.mahle.com/en/products-and-services/e-mobility/thermal-management/[Accessed on: 19 November 2018].

Matadi, Bramy Pilipili et al. (2017): “Irreversible Capacity Loss of Li-Ion Batteries Cycled at Low Temperature Due to an Untypical Layer Hindering Li Diffusion into Graphite Electrode.” In: Journal of The Electrochemical Society, 164 (2017).

Mechler, Gene Collin (2010): Manufacturing and Cost Analysis for Aluminum and Copper Die Cast Induction Motors for GM’s Powertrain and R&D Divisions.

Miller, John M. (2010): Propulsion Systems for Hybrid Vehicles. The Institution of Engineering and Technology.

Miller, TJE (2001): Electronic Control of Switched Reluctance Machines. Newnes.

Mohammed, A.; Djurović, S. (2018): Stator Winding Internal Thermal Stress Monitoring and Analysis Using in-situ FBG Sensing Technology. IEEE Transactions on Energy Conversion.

Naunheimer, Harald et al. (2011): Automotive Transmissions: Fundamentals, Selection, Design and Application. Springer.

Nissan (2018): Nissan e-NV200. Available at: URL: https://www.nissan.it/veicoli/veicoli-nuovi/e-

nv200-evalia.html

Oak Ridge National Laboratory (2013): Battery manufacturing. Available at: URL: https://web.ornl.gov/sci/manufacturing/media/video/

Onda, Kazuo et al. (2006): “Thermal behavior of small lithium-ion battery during rapid charge and discharge cycles.” In: Journal of Power Sources, 158 (2006).

Pavlov, Detchko (2011): Lead-Acid Batteries - Science and Technology - A Handbook of Lead-Acid Battery Technology and its Influence on the Product. Elsevier.

Popescu, Mircea et al. (2016): “Modern Heat Extraction Systems for Electrical Machines – A Review.” In: IEEE Transactions on Industry Applications, (2016).

Rathore, Mahesh M. (2010): Thermal Engineering. Tata McGraw-Hill Education.

Romain, Nicolas (2014): The Nissan e-NV200 battery and electric motor. Available at: URL: http://www.car-engineer.com/nissan-e-nv200-battery-electric-motor/[Accessed on: 25 November 2018].

Schiffer, Michael Brian (2013): The Archaeology of Science: Studying the Creation of Useful Knowledge. Springer International Publishing.

SDP/SI (2018): Gear types and manufacturing.

Shena, Xin et al. (2018): “Beyond lithium ion batteries.” In: Energy Storage Materials, 12 (2018).

Simion, Mihaela; Socaciu, Lavinia; Unguresan, Paula (2016): “Factors which influence the thermal comfort inside of vehicles.” In: Energy Procedia, 85 (2016).

Smith, Robert D.; Peterson, John C. (1998): Mathematics for Machine Technology. Delmar Cengage Learning.

Soares, F.J.; Almeida, P.M. Rocha; Lopes, Joao A. Pecas; Garcia-Valle, Rodrigo; Marra, Francesco (2013): Electric Vehicle Integration into Modern Power Networks. Springer.

Staton, David; Goss, James (2017): Open Source Electric Motor Models for Commercial EV & HybridTraction Motors.

Sun, Jinlei et al. (2014): “LiFePO4 optimal operation temperature range analysis for EV/HEV.” In: International Conference on Life System Modeling and Simulation and International Conference on Intelligent Computing for Sustainable Energy and Environment.

Tesla (2018): Tesla Superchargers in Austria. Available at: URL: https://www.tesla.com/en_GB/findus/list/superchargers/Austria?redirect=no

The AA Motoring Trust (2005): PETROL PRICES 1896 TO PRESENT.

The Editors of Encyclopaedia Britannica (2018): Alessandro Volta - ITALIAN SCIENTIST. Available at: URL: https://www.britannica.com/biography/Alessandro-Volta[Accessed on: 21 November 2018].

TKK Corporation (2018): Nissei Zerol Gears. Available at: URL: https://www.tkkcorporation.com/handling-products/nissei/gears/zerol-gears/[Accessed on: 20 November 2018].

Tong, Wei (2014): Mechanical Design of Electric Motors. CRC Press.

Tort, Oriol Sanfeliu (2016): Design of a Gearbox for an electric FSAE vehicle. Illinois Institute of Technology.

Toyota (2018): Toyota Mirai Brochure. Available at: URL: https://www.toyota.it/gamma/nuova-mirai/perche-idrogeno.json#/ajax/%2Fgamma%2Fnuova-mirai%2Fbrochure.json/[Accessed on: 22 November 2018].

United Nations Climate Change (2018): [No Title]. Available at: URL: https://unfccc.int/process/the-kyoto-protocol[Accessed on: 11 November 2018].

Venn, Fiona (2002): The Oil Crisis. Longman.

Verbrugge, M. W. (1995): "Tree-Dimensional Temperature and Current Distribution in a Battery Module." In: AIChE Journal, 41 (1995).

Vuchic, Vukan R. (2007): Urban Transit Systems and Technology. John Wiley & Sons.

Wang, Qingsong et al. (2014): "A shuttle effect free lithium sulfur battery based on a hybrid electrolyte." In: Physical Chemistry Chemical Physics, 16 (2014).

Wang, Qingsong; Sun, Jinhua; Chu, Guanquan (2015): Lithium Ion Battery Fire and Explosion.

Wertheimer, Eliott (2018): Hydrogen Fuel Cells vs Lithium-ion Batteries in Electric Vehicles. Available at: URL: https://www.furosystems.com/news/hydrogen-fuel-cells-vs-lithium-ion-batteries-in-electric-vehicles/[Accessed on: 12 November 2018].

Whelan, M.; Reilly, Edwin; Rockwell, Steve (2014): Joseph Henry. Available at: URL: http://edisontechcenter.org/JosephHenry.html[Accessed on: 21 November 2018].

Whittingha, Stanley M (1982): Intercalation Chemistry. Academic Press.

Widmer, James D.; Martin, Richard; Kimiabeigi, Mohammed (2015): "Electric vehicle traction motors without rare earth magnets."In: (2015).

Wiebelt, Achim et al. (2009): "Thermomanagement von Lithium-Ionen-Batterien." In: ATZ - Automobiltechnische Zeitschrift, 111 (2009), H. 7–8.

Winnipeg Synthetics (2018): CVT technology and eCVT technology differ greatly. Available at: URL: http://www.winnipegsynthetics.ca/articles/cvt-and-ecvt.html[Accessed on: 20 November 2018].

Yamauchi, Mia (2018): TESLA CHARGING: THE COMPLETE GUIDE TO CHARGING AT HOME, IN PUBLIC AND AUTONOMOUSLY. Available at: URL: https://www.pluglesspower.com/learn/tesla-model-s-charging-home-public-autonomously/

Yamsani, Akilesh (2014): "Gradeability for Automobiles." In: IOSR Journal of Mechanical and Civil Engineering, 11 (2014).

Yang, Yinye; Schofield, N.; Preindl, Matthias (2016): "Thermal management of electric machines." In: IET Electrical Systems in Transportation, (2016).

Yoo, Kisoo et al. (2017): "A Review of Lithium-Air Battery Modeling Studies." In: Energies, 10 (2017).

YUASA (2014): Micro Hybrid & Hybrid Vehicles Explained. Available at: URL: https://www.yuasa.co.uk/info/technical/micro-hybrid-hybrid-vehicles-explained/[Accessed on: 11 November 2018].

7 List of figures

8 List of tables

9 Attachments

9.1 Comparison of properties of materials for the squirrel cage of induction motors [118]

Characteristics	Pure Aluminum[1] *	Ranges for Aluminum Alloys Commonly Used in Cage Construction[1]	Pure Copper[2] **	Ranges for Copper Alloys Commonly Used in Cage Construction[2]
Electrical Conductivity, % IACS @ 20°F	62	34-59	101	7-90
Specific Heat, BTU/Lb. °F. @68° F	0.233	0.233	0.092	0.09
Density, Lb./In.^{3} @68° F	0.098	.097-.098	0.323	.308- .323
Melting Point, °F	1195-1215	1080-1210	1981	1880 2100
Coef. Of thermal expansion,/° C	23.8 x 10^{-6}	23.4-23.6 x 10^{-6}	17.6 x 10^{-6}	17.3-18.7 x 10^{-6}
Coef. Of thermal expansion,/° F	13.2 x 10^{-6}	13.0-13.1 x10^{-6}	9.8 x 10^{-6}	9.6-10.4 x 10^{-6}
Thermal expansion mils/in/100° C	2.38	2.34-2.36	1.76	1.73-1.87
Thermal Conductivity, BTU/Ft.^{2} /ft/hr/° F	135	78-128	226	21-208
Yield Strength, psi x 1000****				
Annealed	4	7-17	10	10-21
Tempered	24	28-40	53	57-80
Ultimate Strength, psi x 1000				
Annealed	12	14-36	32	34-56
Tempered	27	32-45	57	60-92
Elongation, % in 2"				
Annealed	23	22-25	45-55	45-63
Tempered	1.5	10-15	4-40	3-10
Fatigue endurance limit, psi x1000***	7	9-16	11-17	15-31

* Data for Electrical Conductor Grade; 99.45% minimum aluminum.
** Data for CDA Alloy No. 102, Oxygen Free; 99.95% minimum copper.
*** Fatigue limit for aluminum products is based on 500x10^6 cycles. For copper products it is based on 100x10^8 cycles
**** Yield Strength is at 0.2% offset for aluminum products and at 0.5% ext. under load for copper products
Note conductivity is the inverse of resistance

[118] Conf. Finley; Hodowanec (2001), p. 11.

9.2 Summary of selected capacity fade high temperature cycling studies[119]

Author	Materials	DOD range	Cycle rate	Number of cycles	Test temperature	Capacity fade	Power fade	Key conclusions
Ramadass et al.	C/$LiCoO_2$	4.2–2.0 V	*C*/1.8	500	25°C 50°C	22.5% 70.6%		Degradation of negative electrode dominated capacity loss
Ehrlich	C/$LiCoO_2$	4.2–2.5 V	*C*/1	500	21°C 45°C	9.0% 13.0%		
	C/$LiMn_2O_4$	4.2–2.5 V	*C*/1	500	21°C 45°C	28.0% 51.0%		
Amine et al.	MCMB/$LiFePO_4$ ($LiPF_6$ electrolyte)	3.8–2.7 V	*C*/3	100	37°C 55°C	40.0% 70.0%		Dissolution of Fe^{2+} ions high for both coated and uncoated positive electrodes; high temperature capacity fade can be reduced by selecting appropriate electrolyte
	MCMB/$LiFePO_4$ (carbon-coated positive electrode)			50	37°C	40.0%		
	MCMB/$LiFePO_4$ (LiBOB electrolyte)			100	37°C	20.0%		
Liu et al.	C/$LiFePO_4$	90% DOD	*C*/2	2628 757	15°C 60°C	7.5% 20.1%		Capacity fade was primarily due to loss of lithium from repair of SEI on negative electrode; saw no evidence of Fe dissolution in the electrolyte
		50% DOD	6*C*	1376	45°C	22.1%		
Takei et al.	C/$LiCoO_2$	3.1–2.5 V 4.2–3.6 V	Unknown	1500 1300	Unknown	0.0% 40.0%		Capacity fade is a strong function of maximum voltage, especially about 3.92 V
Choi and Lim	C/$LiCoO_2$	4.2–2.75 V 4.2–3.2 V 4.2–3.3 V 4.2–3.4 V 4.2–3.5 V 4.2–3.55 V	*C*/1	500	25°C	13.4% 15.5% 17.0% 15.1% 16.1% 15.8%		No appreciable difference in capacity fade due to increasing DOD
Belt et al.	Unknown	75–75% 75–55% 75–35%	Modified 100 Wh profile	120,000	25°C	7.0% 6.2% 7.1%	15.0% 27.0% 43.0%	Capacity fade is not a strong function of DOD, but power fade is a function of DOD—due to positive electrode breakage
Belt et al.	Proprietary	25 Wh	PNGV cycle-life test protocol	300,000	30°C 40°C 50°C	15.3% 13.7% 11.7%	15.0% 14.5% 16.1%	Capacity/power fade appears to be independent of temperature for small DOD changes for 75% average SOC

[119] Conf. Bandhauer; Garimella; Fuller (2011), p. R2.

9.3 Summary of selected capacity and power fade high temperature storage studies[120]

Author	Materials	Electrolyte	Soak time	Soak temperature	Soak SOC	Capacity fade	Power fade	Key conclusions
Thomas et al.	C/$LiNi_{0.8}Co_{0.15}Al_{0.5}O_2$		35 weeks	25°C	60%		20%	Power fade is primarily temperature dependent in the first 4 weeks, and both time and temperature dependent thereafter
			20 weeks	55°C	100%		55%	
			4 weeks	25°C	60%		3%	
				35°C			3%	
				45°C			7%	
				55°C			12%	
Smart et al.	C/$Li_{1-x}Ni_yCo_{1-y}O_2$	Medium EC electrolyte	10 days	55°C	100%	14%		Capacity fade at high temperatures is strongly dependent on the EC content—more EC results in less capacity fade; capacity fade is more rapid at higher temperatures
		Low EC electrolyte				35%		
		High EC electrolyte	40 days	55°C for 10 days	100%	11%		
				60°C for 10 days				
				65°C for 10 days				
				70°C for 10 days				

[120] Conf. Bandhauer; Garimella; Fuller (2011), p. R3.

9.4 Planetary gear ratio formula derivation

Starting from the previously defined ratio of reduction gear

$$i = \frac{\omega_s}{\omega_c}$$

$$v_c = \omega_c * (r_s + r_p)$$

$$v_s = \omega_s * r_s$$

$$v_s = 2 * v_c = 2 * \omega_c * (r_s + r_p)$$

$$\omega_s * r_s = 2 * \omega_c * (r_s + r_p)$$

$$\frac{\omega_s}{\omega_c} = \frac{2*(r_s+r_p)}{r_s} = \frac{2*r_s+2*r_p}{r_s} = \frac{2*r_s+r_R+r_s}{r_s} = 1 + \frac{r_R}{r_S}$$